DETECTOR AND OTHER INSTRUMENTAL EFFECTS ON SIGNAL-TO-NOISE RATIO IN GAS AND LIQUID PHASE FLUORESCENCE

By

RAYMOND P. COONEY

A DISSERTATION PRESENTED TO THE GRADUATE COUNCIL
OF THE UNIVERSITY OF FLORIDA
IN PARTIAL FULFILLMENT OF THE REQUIREMENTS FOR THE
DEGREE OF DOCTOR OF PHILOSOPHY

UNIVERSITY OF FLORIDA

1977

ACKNOWLEDGMENTS

Those of you to whom I owe a debt of gratitude, for whatever reason, please accept my most sincere and heartfelt thanks.

TABLE OF CONTENTS

Abstract of Dissertation Presented to the
Graduate Council of the University of Florida
in Partial Fulfillment of the Requirements
for the Degree of Doctor of Philosophy

DETECTOR AND OTHER INSTRUMENTAL EFFECTS ON
SIGNAL-TO-NOISE RATIO IN GAS AND LIQUID PHASE FLUORESCENCE

By

Raymond P. Cooney

March, 1977

Chairman: James D. Winefordner
Major Department: Chemistry

Several photomultiplier tubes and image devices (image dissector, silicon vidicon, silicon intensified target vidicon, intensified silicon intensified target vidicon, and secondary electron conduction vidicon) are compared theoretically with respect to signal-to-noise ratio, S/N, in atomic and molecular luminescence spectrometry. Equations describing the S/N for the image devices are developed and compared with the analogous equations for photomultiplier tubes. The equations are then used to calculate S/N for each device under conditions likely to be encountered in analytically important situations. Conclusions based on the calculations include: a) the silicon vidicon is not analytically useful for atomic fluorescence or molecular luminescence spectrometry; b) the image dissector and secondary electron conduction vidicon are possibly useful in atomic fluorescence spectroscopy if used with echelle spectrometers; c) in atomic spectroscopy, whether the optimal

system is an SEC echelle spectrometer, an ID echelle spectrometer, a multichannel direct reader, or slewed scan single channel spectrometer will depend upon how many spectral lines are to be analyzed and whether or not it has been predetermined which lines will be examined; and d) in molecular luminescence spectrometry in the visible (>350 nm), the integrating image devices possess considerable analytical potential, combining a multichannel time advantage with S/N approaching those of photomultiplier tubes.

The feasibility of using an SIT vidicon as a gas phase fluorescence detector for gas chromatography is demonstrated. Gas phase spectra and limits of detection for several polyaromatic hydrocarbons are given, with the SIT having limits of detection about a factor of five larger than those obtained with a photomultiplier (PM) tube (operating in a non-scanning mode).

The feasibility of using the SIT vidicon as a detector for liquid chromatography is also demonstrated. Limits of detection range from $\sim 2 \times 10^{-2}$ ng for anthracene to $\sim 6 \times 10^{-1}$ ng for riboflavin. A direct experimental comparison is made of a multichannel (SIT) and a photomultiplier sequential linear scanning (SLS) system for the detection of steady state fluorescence from molecules in solution. A discussion is given of the fundamental differences between the ways the two systems acquire, process, and read out data. It is concluded that the PM/SLS system is slightly better than the SIT for measuring steady state fluorescence. On the other hand, the multichannel

advantage of the SIT would appear to make it the better system for measuring transient fluorescence signals.

Several different optical systems and excitation sources are compared for the detection of gas phase fluorescence from gas chromatographic eluents. It is determined that, for the systems studied, the limiting noise comes from stray light at the fluorescence emission wavelength which originates at the excitation source and is passed by the system optics and scattered by the sample cell. General conclusions are drawn for improving the system signal-to-noise ratio in the case of either background shot or background flicker noise limitation. For the systems studied, it is concluded that improved performance can be attained by the use of sources with intense output in the far UV or by the use of conventional sources with excitation monochromators which are most efficient in the far UV and have improved (lower) stray light levels.

CHAPTER I
INTRODUCTION

Talmi has recently reviewed the principles of TV-type multichannel detectors (image devices) and their uses in analytical spectroscopy.[1,2] It is quite obvious that multichannel detectors are becoming of greater and greater interest in analytical spectroscopy based upon the applications of such devices in atomic emission spectroscopy, atomic absorption spectroscopy, atomic fluorescence spectroscopy, molecular uv-visible absorption spectroscopy, molecular fluorescence spectroscopy, and Raman spectroscopy.[3-37] These devices are now available as complete detector systems [silicon vidicon (V), silicon intensified target vidicon (SIT), and intensified SIT (ISIT)] from several commercial companies (Princeton Applied Research, Nuclear Data, EMR, RKB, and Quantex). The detector heads and electronic components are also available on a modular basis from several companies (Reticon, GE, Hamamatsu, EMI, Amperex, ITT, RCA, Fairchild, Teltron, TI, and Westinghouse). In addition to the reviews by Talmi, four other review articles have been either partially or totally concerned with image device detectors in atomic spectroscopy.[38-41] In several of the research papers experimental signal-to-noise ratios (S/N), relative standard deviations, and limits of detection for analyte atoms and molecules have been reported. In only

a handful of the research papers, and few of the review papers, have the signal-to-noise ratios been given in terms of the parameters determining them. Indeed, in most of the experimental cases, it is not clear how the S/N ratio has been obtained, i.e., whether the contents of one channel or of many channels are used, and whether there is direct use of information previously stored in digital form or whether the information is converted from digital to analog (graphic) form before use. As a result, it is difficult to compare analytical figures of merit on a systematic basis. In all of the manuscripts considering theoretical expressions for the signal-to-noise ratio, the expressions for signal and noise have been given in analog terms, i.e., currents (rates) rather than in digital terms (counts) despite the fact that digital readout is utilized with all of the image devices. The influence of preamplifier (electronic measurement) noise has been stressed as the most significant noise contribution near the limit of detection while the influence of background luminescence interference, scatter, and dark count noise has usually been neglected. Indeed, there has been no fair comparison, based on calculated signal-to-noise ratios, of the image devices with photomultipliers (PM) or of the image devices with each other.

Therefore, one purpose of this manuscript is to compare the signal-to-noise ratios of several image devices [V, SIT, ISIT, secondary electron conduction vidicon (SEC), and image dissector (ID)] with each other and with several sensitive photomultiplier tubes commonly used in optical spectroscopy.

The comparison is made for several hypothetical, but realistic, experimental situations in atomic and molecular luminescence spectroscopy. The S/N of the image devices are estimated for these realistic experimental conditions either by utilizing the contents of a single channel or by pooling (summing) the contents of several channels (which generally leads to an increase in S/N). Some discussion is also concerned with the calculation of S/N in terms of currents.

In recent years, fluorescence detectors have seen increasing use in liquid and thin layer chromatography. A number of workers have investigated the possibility of using fluorescence detectors in gas chromatography. Bowman and Beroza trapped gas chromatographic eluents in a flowing liquid solvent stream and then monitored the fluorescence as the solvent stream was fed through a spectrophotofluorimeter.[42] Burchfield et al. used a heated transfer line from the gas chromatograph to a heated quartz cell in a spectrophotofluorimeter and observed fluorescence directly in the gas phase.[43] They later modified their system with a gas-phase isolation and injection system in order to analyze polynuclear arenes in air particulates.[44] Freed and Faulkner used a fast scanning fluorescence spectrometer to obtain gas-phase excitation and emission spectra of gas chromatographic eluents.[45] Robinson and Goodbread fabricated a simpler, less expensive, filter fluorimetric detector, useful primarily for quantitative analysis.[46]

A second purpose of this manuscript is to explore the

use of an SIT image device as a gas-phase fluorescence detector for gas chromatography. In previous work, a video fluorometer is described having electronic processing to obtain three-dimensional graphic spectra involving 241 fluorescence spectra at 241 different exciting wavelengths at 16.7 ms per spectrum.[47] In a paper by Vo-Dinh et al., analytical figures of merit, including detection limits, were measured for a commercial spectrophotofluorometer having the photomultiplier-slit arrangement replaced by an SIT (silicon intensified target).[48] In a paper by Dessy et al., a solid state array detector with computer control was used as a molecular absorption spectrophotometric detector for liquid chromatography.[49] In this manuscript, the performance of the SIT image detector is investigated and compared to that of the fast scanning fluorescence spectrometer, especially with regard to the detection of transient signals of gaseous species being eluted from a gas chromatograph; also analytical figures of merit and limitations of the system will be discussed.

In the gas-phase work, anthracene, benzo-[a]-pyrene, chrysene, phenanthrene, and pyrene are studied because they belong to the important class, polynuclear aromatic hydrocarbons (PAHs), which are frequently encountered in air pollutants, urban water, tar, and cigarette smoke.[50] Many PAHs, such as pyrene and benzo-[a]-pyrene have been shown to be highly carcinogenic.

In addition, the performance of the SIT-fluorometer system is studied with regards to the measurement of transient fluorescence emission from molecules in solution, such as would

be the case for detection of fluorescent compounds being eluted from a liquid chromatograph. In addition to several polynuclear aromatic compounds, riboflavine, acridine, and 4,5-diphenylimidazole are studied.

In order to complement the theoretical comparison of image devices and photomultiplier tubes, there is a direct experimental comparison made of the SIT and a sequential linear scanning (SLS) system using a PM for the measurement of steady state fluorescence of molecules in solution. There is also a thorough discussion given of the fundamental differences in the nature of the data and data collecting processes of the two types of detectors.

Finally, there is a critical examination of various systems used for the detection of gas-phase fluorescence signals from gas chromatographic eluents. The aim of this examination is to define precisely the origin and nature of the limiting noise and to show how this information can be used to improve the performance of these systems.

CHAPTER II
THEORETICAL CONSIDERATIONS

In luminescence spectrometry, the analyte luminescence signal S_L is given by

$$S_L = S(L,B,S,I,D) - S(B,S,I,D) \quad (1)$$

where S(L,B,S,I,D) is the signal resulting from the sample and contains contributions resulting from analyte luminescence (L), non-source induced background (B, e.g., flame background emission in atomic fluorescence spectrometry), scatter of source radiation (S), source induced interfering luminescence background (I), and the background resulting from the detector and measurement system (D); and S(B,S,I,D) is the signal resulting from the blank, which ideally is the same in all respects as the signal resulting from the sample except for the absence of analyte luminescence (i.e., no analyte impurity is assumed present in the blank). Assuming negligible statistical dependencies between the noise sources (except for several of the flicker noises discussed below), the total noise due to contributions from all sources is given by

$$N = \sqrt{N_{LS}^2 + 2N_{DS}^2 + 2N_{BS}^2 + 2N_{IS}^2 + [N_{LF} + 2N_{IF} + 2N_{SF}]^2 + 4N_{BF}^2 + 4N_{DF}^2 + 2N_A^2 + 2N_{SS}^2} \quad (2)$$

where the terms are defined as: N_{XS} is the shot noise due to process X (X = L for analyte luminescence, X = D for dark current, X = B for non-source induced background, X = I for source induced background, and X = S for source induced scatter); the corresponding N_{XF} terms represent the flicker type noises associated with the same processes giving rise to the N_{XS} terms; and N_A represents the amplifier-electronic measurement system noises combined into one term.[51,52] It is assumed that the analyte luminescence is present only in measurements made on the sample while all other contributions are present both in measurements made on the sample and (to the same extent) in measurements made on the blank. Thus the coefficients of 1 for N_{LS}^2 and N_{LF}^2 arise from the assumption that analyte luminescence contributes only to the sample signal (and noise). The coefficients of 2 for the other shot noise terms arise from the fact that the shot noise arising from process X measured in the sample, and the shot noise arising from the same process X measured in the blank are independent, and therefore add quadratically. The coefficients of 4 or 2^2 for the corresponding flicker noise terms arise from assuming that the flicker noise arising from process X measured in the sample and the flicker noise arising from the same process X measured in the blank are dependent, and therefore add linearly. In actuality, it is likely that the flicker noises arising from a given process X are to some extent both dependent and independent between sample and blank measurements. However, such considerations are beyond the scope of this paper and even if treated here would result in no significant changes

in the conclusions reached. Chester and Winefordner have considered in detail the influence of the measurement procedure (i.e., the timing between and sequence of sample, blank, and standard measurements) upon the types of noises arising in an analytical procedure.[53] The flicker noises from the analyte luminescence, the interference luminescence, and the scatter are assumed to be dependent (i.e., they all result from flicker in the source) and therefore will add linearly (summed before squaring) to each other.

The signal-to-noise ratio (S/N) expressions below will follow those of the approaches taken by Winefordner et al., in comparing multichannel vs. single channel vs. multiplex methods and by Boutilier et al., in comparing pulsed source/gated detector systems (with and without time resolution) vs. the cw source/cw detector system.[54,55] All calculations in the manuscript will be carried out in terms of total counts (digital) rather than in terms of currents (see Appendix) or in terms of count rates. For non-integrating devices, such as photomultiplier tubes and image dissectors, the integral number of counts in an observation time t_o corresponds to the product of the counting rate due to some process times t_o; while the same is true for integrating devices, such as conventional vidicons (Sb_2S_3 or PbO photoconductors), Si target vidicons, SEC vidicons, and intensified target vidicons (SIT, ISIT or EBS), the observation time is divided into integrating periods (when photon induced charge is stored by the image device) and scanning periods (when the stored charge is read

by an electron beam). Thus, the total observation time is given by

$$t_o = t_s n_s + t_d n_s n_d \quad (3)$$

where

t_s = time per scan, s (32.8 ms for vidicon with PAR-OMA)

t_d = time per integration, s (integrations called delays on PAR-OMA)

n_s = number of scans, dimensionless

n_d = number of integrations (delays) before each scan (from zero to thousands with SEC or cooled vidicons) assumed to be the same for each scan, dimensionless

If $t_d = t_s$, then equation (3) reduces to

$$t_o = t_s n_s (1 + n_d) \quad (4)$$

Generally, the channels of an image device are scanned sequentially, and the number of integrations before each scan is constant. With computer control, it is feasible to have random access channel readout with variable numbers of integrations before a scan.

The signal-to-noise ratio for image devices, $(S/N)_{image}$, is given by

$$(S/N)_{image} = \frac{t_o \Sigma E_{L_i} A_i q_i / \{\sqrt{t_o [\Sigma A_i q_i (E_{L_i} + 2E_{B_i} + 2E_{I_i} + 2E_{S_i}) + 4\Sigma R_{D_i}] + t_o^2 [\Sigma A_i q_i \xi_{S_i} (E_{L_i} + 2E_{I_i} + 2E_{S_i})]^2 + t_o^2 (\Sigma 2A_i q_i \xi_{B_i} E_{B_i})^2 + 2t_o^2 \Sigma (2\xi_{D_i} R_{D_i})^2 + 4\Sigma N_A^2}\}}{} \quad (5)$$

where

E_{X_i} = the photon irradiance in channel i arising from process X (X = L for luminescence irradiance of analyte, X = B for source independent background, X = I for source induced luminescence interference, and X = S for source induced scatter), photons s^{-1} cm^{-2}

ξ_{X_i} = flicker (fluctuation) factor for process X in channel i, dimensionless

A_i = area of channel i, cm^2

q_i = efficiency of conversion of photons to counts in channel i, dimensionless

R_{D_i} = detector dark count rate in half (either upper or lower, as discussed below) of channel i, counts s^{-1}

N_A = preamplifier-electronics noise per half channel i per observation time (as defined in equation (6)), dimensionless (counts)

Σ = summation over the appropriate number of channels

The expressions for the dark current shot noise and for the dark current flicker noise arise because of the manner in which

many of the image devices are normally operated. Generally each channel is divided in half, with radiation striking the "upper" half and no radiation striking the "lower" half. When a channel is read, the contents of the "lower" half (dark current) are subtracted from the contents of the "upper" half (dark current plus photon generated current) so that the counts stored in memory are those resulting from the photon generated current. This subtraction occurs for both the sample and blank measurements. Even though the dark currents in the two channel halves cancel out (ideally), the associated shot noises still add quadratically; the flicker noises are assumed to add linearly over time (i.e., between sample and blank) and quadratically over space (i.e., between channel halves and adjacent channels). Likewise, the preamplifier, which is assumed to be the principle source of electronic measurement noise, operates during the readout of each half channel, and thus will make four noise contributions per channel per pair of sample-blank measurements. Since the preamplifier electronic noises are assumed to be random (rms) noises, the total preamplifier noise is $\sqrt{N_A^2 + N_A^2 + N_A^2 + N_A^2}$ or $\sqrt{4N_A^2}$. Finally, it should be noted that the analyte luminescence, interference luminescence, and scatter flicker noises are all given the same flicker factor, ξ_{S_i}, because they are all assumed to be dependent upon source flicker.

To simplify the S/N calculations, it will be assumed that

(i) the image devices have constant sensitivity and

area over the channels of interest;

(ii) the number of channels of interest, n_c, is determined by the spectral line width or band width or by the spectral bandpass of the spectrometer;

(iii) there is no spreading of a narrow image due to "crosstalk" between channels of the vidicon or due to distortion in the intensifier stage.

For comparison of detectors for luminescence spetrometry, these assumptions should not cause any significant loss of integrity of the results. If the values of A_i and q_i are taken as constant ($A_i = A$; $q_i = q$) over n_c channels, then equation (5) becomes

$$(S/N)_{image} = \frac{t_o A q \Sigma E_{L_i} / \{\sqrt{t_o [A q \Sigma (E_{L_i} + 2E_{B_i} + 2E_{I_i} + 2E_{S_i}) + 4\Sigma R_{D_i}] + t_o^2 A^2 q^2 \{[\Sigma \xi_{S_i} (E_{L_i} + 2E_{I_i} + 2E_{S_i})]^2 + [\Sigma 2 \xi_{B_i} E_{B_i}]^2\} + 2t_o^2 \Sigma (2\xi_{D_i} R_{D_i})^2 + 4\Sigma N_A^2}\ \}}{} \qquad (6)$$

Finally if ξ_{X_i} and E_{X_i} are taken as constants for each process across the n_c channels ($\xi_{X_i} = \xi_X$ and $E_{X_i} = E_X$ and $R_{D_i} = R_D$) then

$$(S/N)_{image} = \frac{t_o A q n_c E_L / \{\sqrt{t_o [A q n_c (E_L + 2E_B + 2E_I + 2E_S) + 4n_c R_D] + t_o^2 A^2 q^2 n_c^2 [\xi_S^2 (E_L + 2E_I + 2E_S)^2 + (2\xi_B E_B)^2] + 8t_o^2 n_c \xi_D^2 R_D^2 + 4n_c N_A^2}\ \}}{} \qquad (7)$$

The detector dark count rate varies greatly with the type of detector employed, e.g., SEC vidicons have a dark count rate thousands of times smaller than Si vidicons, SITs, ISITs, or similar devices. The dark count rate of image devices can be reported either in terms of accumulation rate (see Appendix) or in terms of readout rate (as found in most technical and commercial literature). The ratio of readout rate to accumulation rate is equal to the ratio of accumulation time to readout time. If there are no delays between scans, the readout rate per channel (or half channel if the target is divided in half to correct for dark current) is approximately the number of channels (or half channels) times the accumulation rate per channel (or half channel), e.g., for the PAR system, the dark current in each half channel accumulates over 32.8 ms, and is read out in 32.8 μs, and so the readout rate is 1000 times the accumulation rate. The number of preamplifier noise counts, N_A, is determined by Johnson noise within resistive components of the electronic measurement circuits and by the equivalent target electron uncertainty per channel. At the "state of the art," 1000 to 3000 electron rms (depending on the measurement system) are needed to produce one count. An estimate of the preamplifier noise N_A (in counts) is given by

$$N_A = N_a\sqrt{n_s} = N_a\sqrt{t_o/(t_s + n_d t_d)} \qquad (8)$$

where N_a is the preamplifier equivalent noise per half channel

per scan in rms counts and all other terms have been previously defined.

The signal-to-noise ratio for photomultiplier tubes and image dissectors $(S/N)_{PM}$ is given by

$$(S/N)_{PM} = \frac{t_o\, dAqE_{pL}/\{\sqrt{t_o[Aq(dE_L + 2dE_I + 2dE_S + 2E_B) + 2R_D] + t_o^2A^2q^2d^2[\xi_S^2(E_L + 2E_I + 2E_S)^2 + (2\xi_BE_B)^2] + (2\xi_DR_D)^2 + 2N_A^2}\}}{} \qquad (9)$$

where all irradiance terms are as defined above, i.e., for the PM, they correspond to the appropriate irradiance reaching the detector (surface area of photomultiplier and image dissector is A and the detector photon to count efficienty is q). R_D is the photomultiplier or ID dark count rate, s^{-1}, and N_A is the preamplifier electronic measurement noise (counts) which for PM's and ID's will be negligible in all cases with modern electronic measurement systems (except possibly for the case of low dark current due to cooling while at the same time measuring very low irradiances from all processes). The term d is the duty factor for a system where the light source is modulated (d = 1 for an unmodulated source).

CHAPTER III
EXPERIMENTAL

Discussion of the experimental procedures is divided into five separate sections, each with a corresponding section in the chapter dealing with results and discussion.

Signal-to-Noise Ratio Calculations

Signal-to-noise ratio calculations are made for atomic and molecular luminescence spectroscopy with the V, SIT, ISIT, ID, SEC, and with photomultiplier detectors utilizing equations (5) and (9). In Table I, a comparison of detectors is given. Calculations were performed for several realistic experimental situations; in atomic fluorescence spectrometry for both image devices and photomultiplier tubes $E_L = 10^5$ or 10^7 photons cm^{-2} s^{-1}; E_B, E_I, and $E_S = 10^3$ or 10^7 photons cm^{-2} s^{-1}; $\xi_S = 0.003$ and $\xi_B = 0.01$ for image devices and $\xi_S = 0.003$ and $\xi_B = 0.00$ for photomultiplier devices due to modulation with phase sensitive (lock-in) or synchronous photon counting detection; in molecular luminescence spectrometry for both the image devices and the photomultipliers, $E_L = 10^4$ or 10^6 photons cm^{-2} s^{-1}; E_S and $E_I = 10^2$ or 10^6 photons cm^{-2} s^{-1}; $\xi_S = 0.003$. All counting rates for analyte luminescence, source induced luminescence, background, and scatter were calculated from the photon

TABLE I
COMPARISON OF DETECTORS

Parameter[a]	SiVidicon[b,c]	SIT[b,c]	ISIT[b,c]	SEC-Vidicon[b,c]	Image Dissector[b,c]
Internal gain	~1	$\sim 10^3$	$\sim 2\times10^3$	$\sim 10^2$	$\sim 10^6$
Efficiency, q (maximum)	2×10^{-4}	5×10^{-2}	1×10^{-1}	5×10^{-3}	2×10^{-1}
Dark count rate (20°C) (s^{-1})[e]	5	5	5	$<1\times10^{-2}$	$<1\times10^{-1}$
Area per channel (cm^2)[f]	1×10^{-3}	1×10^{-3}	1×10^{-3}	1×10^{-3}	$<1\times10^{-4}$

[a] Parameters: gain = number of charged pairs produced at target (V, SIT, ISIT, SEC) or electrons produced
q is as defined in text
count rate = photon flux x channel area x efficiency (q)
dark count rate = dark counts per second per channel for image devices

[b] Data taken from: OMA Catalog, Princeton Applied Research, Princeton, NJ

[c] Data taken from: The Optical Data Digitizer - An Applications Guide, EMR Schlumberger, Princeton, NJ; Y. T. Talmi, Anal. Chem., 47, 697A (1975).

[d] Data taken from: EMI Catalog, EMI Electronics, Ltd., Middlesex, 6B3,1HJ, England
ITT Catalog

[e] Dark count rates are defined for an entire channel. On some commercial devices half the tube face is blocked off and used for automatic dark current subtraction; thus for half a channel which is illuminated, the dark count rate will be one-half of those in this table

[f] Area per channel for SiVidicon, SIT and ISIT taken from PAR data; area per channel for SEC-Vidicon taken from Talmi; area for image dissector taken as area of aperture; area for PM is same as slit area as long as slit area <<area of photocathode

TABLE I - continued

Parameter[a]	PM(6256EMI)[d]	PM(9558EMI)[d]	PM(FW130ITT)[d]
Internal gain	$\sim 10^{7}$	$\sim 10^{7}$	$\sim 10^{7}$
Efficiency, q (maximum)	2×10^{-1}	2×10^{-1}	2×10^{-1}
Dark count rate (20°C) (s^{-1})[e]	1×10^{2}	1×10^{4}	5×10^{0}
Area per channel (cm^2)[f]	-	-	-

irradiances given in Tables II and III at the maximum quantum efficiency for each detector (peak of spectral response curve); therefore, the S/N will be the same or less at any other wavelength. No effort was made to account for the variation in response with position (channel) for integrating image devices because it was assumed that all channels have equivalent sensitivities ($q_i = q$ = constant). Experimental conditions range from low to high analyte signal levels with the presence of low to high noise due to the preamp, detector, and photon shot and/or flicker noises due to non-analyte photon irradiances (interference, scatter, and background). All S/N calculations were performed for two measurement times, t_o = 1.05 s or 32.8 s. In addition for the V, SIT, ISIT, and SEC integrating image devices (target integration), S/N calculations for a given t_o were done both for the case of no delays, i.e., each scan begins immediately upon completion of the previous scan, and for the case of 3 delays, i.e., for 3x0.0328 s between the end of one scan and the beginning of the next. Because the SEC has "no" dark current and is strictly an integrating device, it is assumed to be read out only after either 1.05 s or 32.8 s. Finally, with the V, SIT, ISIT, and SEC in atomic fluorescence, it is assumed that four channels of the device are illuminated with the spectral line image (four channels have a width of 100 μm corresponding to the slit width used in the atomic fluorescence with photomultiplier calculations) and the S/N is calculated for both the case of one of the channels measured and the case of all four of the channels summed. Similarly,

with the V, SIT, ISIT, and SEC in molecular luminescence spectrometry, it is assumed that forty channels of the image device (1 mm) are covered by the spectral bandwidth of the spectrometer, and the S/N is calculated for the two cases of one channel and forty channels summed.

Other experimental conditions including area of channels V, SIT, ISIT, and SEC, area of aperture of ID, illuminated area of PM, preamp noise, cycle (scan) times for the image devices, etc., are listed in the footnotes of Tables II and III, as well as in Table I.

It should be stressed that the S/N calculations were not made to describe formally any actual experimental situations in atomic fluorescence spectrometry or molecular luminescence spectrometry. However, the hypothetical cases chosen in Tables II and III do represent possible analytically important situations, and more importantly they represent several limiting situations indicating the general usefulness of various types of detectors. In addition, although S/N calculations were carried out only for atomic and molecular luminescence spectrometry, many of the calculations and especially the conclusions (next section) also apply to atomic and molecular absorption and to atomic and molecular emission spectrometry, especially if the appropriate values of parameters are chosen. For example, in atomic and molecular emission spectrometry, the S/N calculations are identical to those for atomic fluorescence except that the background flicker contribution (even with a photomultiplier assuming no sample modulation) is

significant, i.e., $\xi_B \gtrsim 0.01$. In absorption spectrometry much greater spectral irradiances reach the detector even when using lower intensity and higher stability sources (such as hollow cathode lamps in atomic absorption spectrometry). Photon flicker noises are often quite small (because $\xi_S < 0.001$), and so such systems are often photon shot noise limited.

Gas Phase Fluorescence Detection with the SIT

Apparatus

A Model 1400, gas chromatograph (Varian Instrument Division, Palo Alto, CA) was employed in the work. Because evaluation of the detector was the sole object of the study, no actual chromatographic separations were carried out; a 3 ft length of 1/8 in o.d. stainless steel tubing was used to simulate a chromatographic column. The chromatograph was connected to the SPF with an 1.5 ft length of 1/16 in o.d. stainless steel transfer line. The transfer line was heated by means of a 1 in x 4 ft heating tape (Briscoe Manufacturing Company, Columbus, OH); the temperature was controlled by a variable autotransformer (Staco Inc., Dayton, OH) and monitored with a calibrated iron-constantan thermocouple. The heating tape was covered with several layers of asbestos and aluminum foil. Samples were injected with a 10 µl syringe (Hamilton Company, Reno, NV).

The gas phase fluorescence analysis system consisted of an Aminco spectrophotofluorimeter (SPF) (American Instrument

Company, Silver Spring, MD) which was adapted to the analysis of gas chromatographic eluents. The excitation light source was a 150 W Eimac xenon arc lamp regulated by a Varian dc power supply (Model 250S-2, Varian, Eimac Div., San Carlos, CA). This source has been shown to improve limits of detection of condensed phase molecular luminescence by almost an order of magnitude.[56] A lens and a spherical mirror were used to divert the exciting light beam into the entrance slit of the f/4 Czerny-Turner type excitation monochromator. A schematic diagram of the experimental arrangement is given in Figure 1.

The gas flow cell was a 50 mm long rectangular quartz cell (Aminco, type B16-63019) having 3 mm and 5 mm internal and external diameter, respectively. The cell was inserted inside the SPF cell compartment which had been modified to contain a heated brass block which was bored to hold the gas cell and two cartridge heaters (Model 60213, General Electric). The heater output was controlled by an autotransformer (Superior Electric Company, Bristol, CT). The cell temperature was varied between 200 and 280°C and was measured with another calibrated iron-constantan thermocouple. The sample compartment base plate and cover were made from asbestos to insulate the adjacent SPF monochromators from heat generated by the cell holder. Fans were used to keep the two SPF monochromators at 30-40°C under operating conditions. Because scattered light was a critical factor, it was desirable to use monochromator slit widths smaller than the cell dimensions. On the other hand, a decrease in the slit widths necessarily leads to

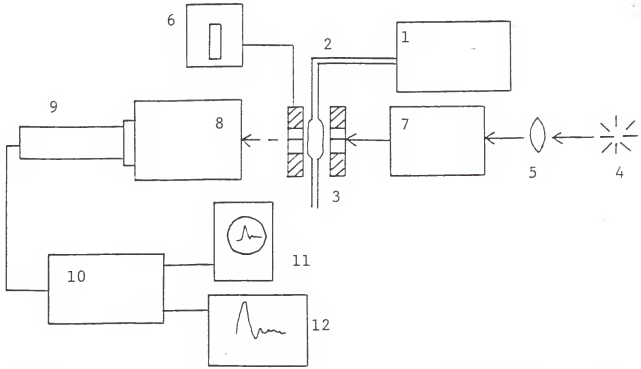

Figure 1. Block Diagram of the Gas Chromatograph and the Fluorimeter-SIT Image Detector.

1. Gas chromatograph
2. Transfer line
3. Flow cell
4. Light source
5. Optics
6. Heating device
7. Excitation monochromator
8. Emission monochromator
9. SIT image converter
10. Optical multichannel analyzer
11. Oscilloscope
12. Strip chart recorder

smaller signal strengths. Although larger slits would lower the limits of detection (discussed in a later section), slit widths of 2 mm in the excitation path and 1 mm in the emission path were chosen in order to provide a 5 nm spectral resolution.

The detection device consisted of a silicon-intensifier-target (SIT) camera tube (Model 12Q5, Princeton Applied Research, Princeton, NJ). The SIT device was mounted directly on the exit of the analyzing (emission) monochromator of the SPF, and the standard slit assembly and the photomultiplier were removed. The 12.5 mm wide SIT target, having 500 elements or channels allowed multichannel detection over a selectable spectral interval of 62.5 nm. An optical multichannel analyzer (OMA, Model 1205 D, Princeton Applied Research) recorded the data which could be stored in either of two 500 word 21 bit memories (memory "A" or "B"). The SIT/OMA system has the capability to perform the following operations:

(i) In the "real time mode", detection and recording in memory A, a temporally changing signal and display on an oscilloscope after each machine cycle (32.8 ms).

(ii) Integration of data on all 500 channels for a specified time period determined by a selectable number of presets (0 - 9999) and delays (0 - 9). In all cases, delay of 0 was used.

(iii) Storage of the integrated data either in memory A or B.

(iv) Subtraction of the stored data from one another (A - B).

(v) Provision of a digital display of the signal magnitudes and their corresponding spectral positions (channel number).

(vi) Summation of the magnitudes of the signals between specified spectral ranges (peak areas).

(vii) Provision of an analog output which could be used to record the spectra on a chart recorder.

In most of the experiments, the luminescence signal plus background (scattered light, dark signal) were stored in memory A and the background alone in memory B. The background corrected signal A - B which we was of main interest was visually displayed on an oscilloscope (Model 1220A, Hewlett Packard) and read out by a strip chart recorder (Model SRG, Sargent Welch Scientific, Skokie, IL).

Reagents

The polynuclear arenes employed were anthracene and pyrene (Chem Service, West Chester, PA), phenanthrene (Eastman Organic Chemicals, Rochester, NY), chrysene and benzo-[a]-pyrene (Research Organic/Inorganic Chemical Corp., Sun Valley, CA). The solvent used was cyclohexane (Reagent ACS, Matheson Coleman & Bell, Norwood, OH).

Procedure

The Eimac xenon arc lamp, the SPF, the gas chromatograph, and the SIT/OMA system were operated according to the manufacturer's instructions and as discussed previously by Vo-Dinh, Johnson, and Winefordner.[47]

Condensed Phase Fluorescence Detection with the SIT

Apparatus

A block diagram of the instrumental system is shown in Figure 2. Most of the equipment is the same as that used in the gas phase work, i.e., the source, spectrometer, flow cell, SIT/OMA, oscilloscope, chart recorder, and syringes.

For this study, a system simulating a liquid chromatograph was built. The system was designed to be simple and practical, its sole purpose being to provide a flow of solvent with which to carry injected samples to and through the detector. The pump was a peristaltic design (Ismatac, Saia Ag., Murten, Switzerland, type AMY8-D-25SR). This type of pump produces a pulsating flow, however, this did not affect the performance of the SIT due to the fact that, being an integrating detector, it is not flow sensitive. The injection port was constructed from a 1/8 in Swagelok Union Tee fitting and inserted between the pump and the flow cell. Solvent was fed into the branch portion of the union tee (see Figure 1), while samples were injected through a rubber septum placed inside one of the hex nuts on the run portion of the union tee. This arrangement, as opposed to injecting through the branch portion of the union tee, allowed the sample to enter the solvent stream past the right angle bend, thus avoiding possible sample hang-up and excessive band broadening. Tygon 1/8 in o.d. tubing was used between the solvent reservoir and the pump, and between the pump and the injection port, while 1/8 in o.d.

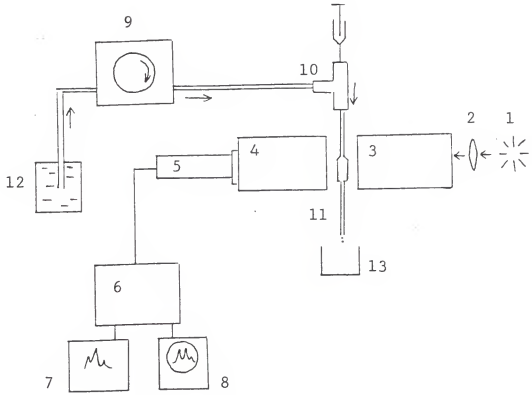

Figure 2. Block Diagram of the Flow Cell and SIT/OMA Detection System for Condensed Phase Studies

1. Light Source
2. Optics
3. Excitation monochromator
4. Emission monochromator
5. SIT image vidicon
6. Optical multichannel analyzer
7. Strip chart recorder
8. Oscilloscope
9. Peristaltic pump
10. Injection port
11. Flow cell
12. Carrier solvent reservoir
13. Carrier solvent collector

Teflon tubing was used between the injection port and the flow cell.

Reagents

Deionized water and spectrograde methanol (Matheson Coleman & Bell, Norwood, OH) were used as solvents. The compounds studied, without further purification were perylene, anthracene (Chem Service, West Chester, PA), chrysene, benzo-[a]-pyrene (Research Organic/Inorganic Chemical Corp., Sun Valley, CA), riboflavine (National Biochemicals Co., Cleveland, OH), acridine (Eastman Organic Chemicals, Rochester, NY), and 4,5-diphenylimidazole (Aldrich Co., Milwaukee, WI).

Procedure

Samples were injected after a uniform rate of sample flow had been established. The first few injections of each compound were made at sufficiently large concentrations ($\geq$100 ppm) so that real time signals could be observed on the oscilloscope output of the OMA. This allowed direct measurement of both the elution time and the sample peak width. Once the real time signal appeared on the scope, the solvent flow could be stopped (by temporarily turning off the pump), allowing the excitation and emission monochromators to be adjusted for maximum signal intensity and optimum placement of the emission spectrum in the ~62 nm spectral window of the system. Subsequently, sample concentrations were reduced by a factor of 100 or more in order to determine limits of detection. Generally, data were accumulated over the entire sample peak width.

Comparison of SIT and SLS

Apparatus

The apparatus used in the comparison study was generally the same as that listed above in the condensed phase fluorescence section. However, in the comparison studies, the flow cell was replaced by a standard 10 x 10 mm i.d. Spectracil quartz cuvette, and the SIT was used alternately with a Hamamatsu 1P21 photomultiplier (PM) tube. Signals from the PM were processed by an O'Haver type nanoammeter.[57]

Reagents

The anthracene used without further purification was obtained from Chem Service, West Chester, PA. The cyclohexane also used without further purification was Reagent ACS, Matheson Coleman & Bell, Norwood, OH.

Procedure

It was desired to make the spectral bandwidths of both systems the same; therefore, the arrangement and sizes of the slits were the same in both the SLS and SIT cases, with one exception. In the SIT case, the exit slit of the emission monochromator was removed and the camera placed at the focal plane, so that a 1:1 image of the limiting entrance slit was formed on the detector face. The spectral bandwidth used was 10 nm, because narrower bandwidths would have decreased sensitivity without improving resolution due to the broad band-

widths of the anthracene spectrum. Because measurements were made by both systems on the same solution, the spectral irradiancies to both detectors were the same.

Observations of sample and blank with the SIT were made for 1000 accumulation cycles each, or 65.6 s, and covered a spectral window of 62 nm. The OMA printed the contents of its 500 channel memory (62 nm window) in 131 s, or at a rate of one channel per 0.26 s (or 0.47 nm s^{-1}). The PM system scanned and printed a 62 nm window in 32 s, or at a rate of 1.9 nm s^{-1}.

In order for the noise bandwidth, Δf, of both systems to be the same ($\Delta f_{SIT} = 1/2t_o = 1/2x65.5$ s $= 7.6x10^{-3}$ Hz, where t_o is the observation time, s; $\Delta f_{SLS} = 1/4\tau = 1/4x0.5$ s $= 0.5$ Hz, where τ is the electronic time constant of the system), τ for the PM system would have to have been 32.8 s. However, it was decided to set τ equal to 0.5 s because this is a value typically used in dc systems (τ's on the order of half a minute are not ordinarily available with commercial instruments), and because a time constant of 0.5 s was compatible with the ~2 nm s^{-1} scan rate, which was chosen so that the SLS system's scanning time and the SIT system's observation time of the 62 nm window would be the same.

The spectra obtained with both systems were printed using the same chart recorder ($\tau = 0.1$ s, $\Delta f = 2.5$ Hz). Signal-to-noise ratios (S/N) and limits of detection were calculated with the data obtained from the printed spectra.

Instrumental Effects on S/N

Apparatus

For the comparison studies reported in this work, several combinations of optical components and excitation sources were employed. In all the studies the gas chromatograph used was as described above; the sample compartment was the flow cell described above; the photomultiplier tube was a Hamamatsu 1P21 (Hamamatsu Corp., Middlesex, NJ); in the dc systems, signals from the PM were fed to an O'Haver type nanoammeter, and in the pulsed systems, signals were processed by a boxcar integrator (Model 160, Princeton Applied Research Corp., Princeton, NJ); signals from the nanoammeter and boxcar integrator were recorded by a strip chart recorder (Model SRG, Sargent Welch Scientific, Skokie, IL).[57]

Figure 3 shows a block diagram of systems i, ii, and iii, consisting of the gas chromatograph connected by a heated transfer line to the quartz flow cell, held in a modified heated cell compartment of an Aminco spectrophotofluorimeter, i.e., the same system described earlier. The only modifications made in this study were in the excitation sources, which were: in system i a 150 W Eimac xenon arc lamp (Varian Eimac Div., San Carlos, CA) was operated in a continuous (cw) mode at 11.5 A dc with a Varian power supply (Model 2505-2); in system ii, the 150 W Eimac lamp was operated in a pulsed mode, using a pulsed power supply (Velonix, Div. of Pulse Engineering, Inc., Santa Clara, CA); and in system iii, a 200 W Hanovia mercury-xenon arc lamp was operated cw at 150 W with a standard

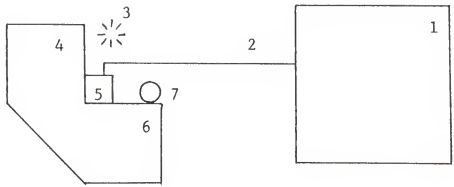

Figure 3. Block Diagram for Systems i, ii, and iii.

1. Gas chromatograph
2. Heated transfer line
3. Light source (see text)
4. Excitation monochromator
5. Sample (flow) cell
6. Emission monochromator
7. Photomultiplier tube

Aminco power supply, and was placed in a standard Aminco ellipsoidal condensing system.[58] Figure 4 shows a block diagram for systems iv and v. In both of these cases, the quartz flow cell was placed in the oven of the gas chromatograph, and was connected to the simulated column by means of a short length of 1/8 in o.d. Teflon tubing, using 1/8 in swagelock fittings with Teflon and Vespel fittings with the Teflon tubing and flow cell, respectively. Holes were drilled through the chromatograph oven wall to pass the exciting and emitted radiation. Quartz windows were placed in the holes to retard heat loss from the oven. Quartz lenses were used to focus light to and from the cell. Pairs of baffles with 2 mm slits were placed near the cell in the excitation and emission paths to reduce scattered light. The emission monochromator (Model 33-86-25-02, Bausch & Lomb Inc., Rochester, NY) for systems iv and v was blazed at 500 nm and had a linear dispersion of 6.4 nm/mm.

In system iv, the excitation source was an Avco Pulsed Nitrogen Laser (Model C950, Avco Everett Research Laboratory, Everett, MA). The laser output was reflected off two mirrors before being focussed into the flow cell. In system v, the excitation source was a 150 W Eimac xenon arc lamp operated in the cw mode. The excitation monochromator was blazed at 250 nm with a linear dispersion of 3.2 nm/mm (Model 33-86-25-01, Bausch & Lomb).

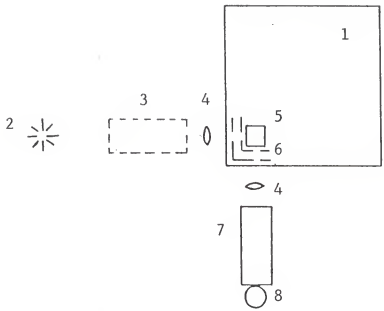

Figure 4. Block Diagram for Systems iv and v.

1. Gas chromatograph
2. Light source (see text)
3. Excitation monochromator
4. Lens
5. Sample (flow) cell
6. Baffles
7. Emission monochromator
8. Photomultiplier tube

Reagents

The polynuclear arenes employed (without further purification) were anthracene and pyrene (Chem Service, West Chester, PA), phenanthrene (Eastman Organic Chemicals, Rochester, NY), and chrysene (Research Organic/Inorganic Chemical Corp., Sun Valley, CA). The solvent was cyclohexane (Reagent ACS, Matheson Coleman & Bell, Norwood, OH).

Procedure

Temperature. In all cases, the injection port temperature was 270°C. In systems i, ii, and iii, the oven and transfer line temperatures were 300°C, and the flow cell temperature was 280°C. In systems iv and v, the oven (and cell) temperature was 240°C.

Pulsed System. The Eimac xenon arc lamp was pulsed at a rate of 150 Hz, with a pulse width of 42 μs, and a peak voltage of approximately 40 V. The boxcar integrator was adjusted for maximum signal amplitude.

Limits of Detection. In all cases, for each compound, at least five injections were made at several combinations of excitation and emission wavelengths in order to determine their optimum values. The limit of detection was calculated as the amount of material, in g, which would give a signal (peak height)-to-noise (rms) ratio of 3.

Source Scatter Study. The emission monochromator was set to 370 nm and the setting of the excitation monochromator was varied (235, 255, and 275 nm). At each setting of the

excitation monochromator, the background signal (in A) was measured with and without an interference filter placed in between the flow cell and the exit slit of the excitation monochromator (system v). The transmittance of the filter was 9% at 370 nm and 0.01% at 235, 255, and 275 nm.

Noise vs. Background Intensity. With the flow cell in place (system v), the emission monochromator was set at 400 nm. The wavelength setting of the excitation monochromator and the slit widths of both monochromators were adjusted to give the desired background signal level. This background signal was fed to the chart recorder, and the noise on the background was taken off the chart recording; rms noise was taken as one fifth the peak-to-peak noise.

Flow Rate. In all cases, the carrier gas (N_2) flow rate was adjusted so that the peak width at half height for anthracene, phenanthrene, and chrysene was 3 s, and for pyrene was 4 s.

Photomultiplier. In all cases, the PM applied voltage was 600 V.

Slit Width. In systems i, ii, and iii, slit widths immediately adjacent to the flow cell were 2 mm and 1 mm on the excitation and emission sides, respectively. The entrance and exit slit widths of the excitation and emission monochromator were 5 mm. For systems iv and v the entrance and exit slit widths of the emission monochromator were 1.5 mm and 6 mm, respectively. For system v, the excitation monochromator had entrance and exit slit widths of 6 mm and 3 mm, respectively.

Time Constant. All systems had a limiting time constant of 0.5 s.

CHAPTER IV
RESULTS AND DISCUSSION

Signal-to-Noise Ratio Calculations

The results of the S/N calculations are in Tables II and III, and can be summarized as shown below. Specific conclusions regarding certain experimental conditions can be determined by looking at the results in Tables II and III or by calculation of S/N via equations (5) and (9). The following symbols will be used throughout the discussion for comparison of signal-to-noise ratios for the detectors considered.

- >> means greater than a factor of 10 (usually greater than 100).
- > means a factor of 2 to 10.
- ≳ means within a factor of 2.

General Conclusions (Common to both Atomic and Molecular Luminescence Spectrometry)

(i) For integration times less than about 0.4 s [12 integrations (delays)] at 32.8 ms per integration (delay) preamplifier noise for image devices dominates over dark current shot noise. The preamplifier noise can be reduced by the factor $\sqrt{1 + n_d}$, where n_d is the number of delays (integrations; if $n_d = 0$, this implies for the PAR/OMA that the time between

TABLE II
SIGNAL-TO-NOISE RATIOS FOR ATOMIC FLUORESCENCE SPECTROMETRY

Conditions				Single Channel Devices[c]							
				Photomultiplier Tubes[d] with Synchronous Photon Counter						Synchronous Photon Counter	
Device				EMI 9558Q		EMI 6256S		ITT FW130		Image[e] Dissector	
Count Time, s[a]				1.05	32.8	1.05	32.8	1.05	32.8	1.05	32.8
$\log E_L$	$\log E_B$	$\log E_S$	$\log E_I$[b]								
5	3	3	3	0.72	4.0	5.8	32.0	9.4	52.0	0.91	5.1
5	3	3	7	0.49	1.4	0.66	1.5	0.66	1.5	0.07	0.39
5	3	7	3	0.49	1.4	0.66	1.5	0.66	1.5	0.07	0.39
5	3	7	7	0.37	0.78	0.43	0.80	0.44	0.80	0.05	0.27
5	7	3	3	0.42	2.3	0.51	2.9	0.51	2.9	0.05	0.29
5	7	3	7	0.35	1.3	0.40	1.4	0.41	1.4	0.04	0.23
5	7	7	3	0.35	1.3	0.40	1.4	0.41	1.4	0.04	0.23
5	7	7	7	0.30	0.76	0.33	0.77	0.33	0.77	0.04	0.20
7	3	3	3	58.0	230.0	97.0	290.0	98.0	290.0	10.0	56.0
7	3	3	7	42.0	100.0	52.0	110.0	52.0	110.0	5.9	31.0
7	3	7	3	42.0	100.0	52.0	110.0	52.0	110.0	5.9	31.0
7	3	7	7	33.0	64.0	38.0	65.0	38.0	65.0	4.6	24.0
7	7	3	3	38.0	180.0	45.0	200.0	45.0	200.0	4.6	26.0
7	7	3	7	33.0	96.0	37.0	99.0	37.0	99.0	3.9	21.0
7	7	7	3	33.0	96.0	37.0	99.0	37.0	99.0	3.9	21.0
7	7	7	7	28.0	62.0	30.0	63.0	30.0	63.0	3.4	18.0

TABLE II - continued

Conditions				Multichannel Image Devices[c,f]							
				4 Channels Illuminated with One Channel Measured							
				No Integration							
Device				V		SIT		ISIT		SEC[g]	
Count Time, s[a]				1.05	32.8	1.05	32.8	1.05	32.8	1.05	32.8
log E_L	log E_B	log E_S	log[b] E_I								
5	3	3	3	0.002	0.01	0.54	3.0	1.1	5.9	1.9	12.4
5	3	3	7	0.002	0.01	0.17	0.83	0.25	1.1	0.16	0.79
5	3	7	3	0.002	0.01	0.17	0.83	0.25	1.1	0.16	0.79
5	3	7	7	0.002	0.01	0.12	0.53	0.17	0.64	0.11	0.51
5	7	3	3	0.002	0.01	0.16	0.44	0.22	0.47	0.15	0.44
5	7	3	7	0.002	0.01	0.12	0.39	0.17	0.43	0.11	0.38
5	7	7	3	0.002	0.01	0.12	0.39	0.17	0.43	0.11	0.38
5	7	7	7	0.002	0.01	0.10	0.34	0.14	0.38	0.09	0.33
7	3	3	3	0.22	1.2	23.0	120.0	34.0	170.0	23.0	120.0
7	3	3	7	0.22	1.2	14.0	65.0	20.0	80.0	13.0	62.0
7	3	7	3	0.22	1.2	14.0	65.0	20.0	80.0	13.0	62.0
7	3	7	7	0.21	1.2	11.0	46.0	16.0	53.0	10.0	43.0
7	7	3	3	0.22	1.2	14.0	42.0	19.0	45.0	13.0	41.0
7	7	3	7	0.21	1.2	11.0	37.0	15.0	41.0	10.0	36.0
7	7	7	3	0.21	1.2	11.0	37.0	15.0	41.0	10.0	36.0
7	7	7	7	0.21	1.2	9.3	32.0	13.0	36.0	8.5	31.0

TABLE II - continued

Conditions				Multichannel Image Devices[c,f]					
				4 Channels Illuminated with One Channel Measured					
				0.0984 s Integration					
Device				V		SIT		ISIT	
Count Time, s[a]				1.05	32.8	1.05	32.8	1.05	32.8
log E_L	log E_B	log E_S	log[b] E_I						
5	3	3	3	0.004	0.02	0.93	5.2	1.7	9.8
5	3	3	7	0.004	0.02	0.18	0.85	0.25	1.1
5	3	7	3	0.004	0.02	0.18	0.85	0.25	1.1
5	3	7	7	0.004	0.02	0.13	0.54	0.18	0.64
5	7	3	3	0.004	0.02	0.17	0.45	0.23	0.47
5	7	3	7	0.004	0.02	0.12	0.39	0.17	0.43
5	7	7	3	0.004	0.02	0.12	0.39	0.17	0.43
5	7	7	7	0.003	0.02	0.10	0.34	0.14	0.38
7	3	3	3	0.39	2.2	25.0	130.0	35.0	170.0
7	3	3	7	0.37	2.1	15.0	66.0	20.0	80.0
7	3	7	3	0.37	2.1	15.0	66.0	20.0	80.0
7	3	7	7	0.35	2.0	11.0	46.0	16.0	54.0
7	7	3	3	0.37	2.1	14.0	42.0	19.0	46.0
7	7	3	7	0.35	2.0	11.0	37.0	15.0	41.0
7	7	7	3	0.35	2.0	11.0	37.0	15.0	41.0
7	7	7	7	0.33	1.9	9.4	32.0	13.0	35.0

TABLE II - continued

Conditions				Multichannel Image Devices[c,f]							
				4 Channels Illuminated with 4 Channels Measured[h]							
				No Integration							
Device				V		SIT		ISIT		SEC[g]	
Count Time, s[a]				1.05	32.8	1.05	32.8	1.05	32.8	1.05	32.8
log E_L	log E_B	log E_S	log[b] E_I								
5	3	3	3	0.004	0.02	1.1	6.1	2.1	12.0	3.8	25.0
5	3	3	7	0.004	0.02	0.34	1.3	0.48	1.4	0.32	1.2
5	3	7	3	0.004	0.02	0.34	1.3	0.48	1.4	0.32	1.2
5	3	7	7	0.004	0.02	0.24	0.71	0.33	0.77	0.22	0.70
5	7	3	3	0.004	0.02	0.28	0.48	0.38	0.49	0.27	0.48
5	7	3	7	0.004	0.02	0.22	0.45	0.29	0.47	0.21	0.45
5	7	7	3	0.004	0.02	0.22	0.45	0.29	0.47	0.21	0.45
5	7	7	7	0.004	0.02	0.19	0.40	0.24	0.41	0.17	0.40
7	3	3	3	0.44	2.5	46.0	210.0	67.0	250.0	45.0	200.0
7	3	3	7	0.43	2.4	28.0	91.0	39.0	100.0	26.0	89.0
7	3	7	3	0.43	2.4	28.0	91.0	39.0	100.0	26.0	89.0
7	3	7	7	0.43	2.4	21.0	59.0	29.0	62.0	20.0	58.0
7	7	3	3	0.43	2.4	25.0	47.0	32.0	48.0	23.0	47.0
7	7	3	7	0.43	2.4	20.0	43.0	26.0	44.0	19.0	42.0
7	7	7	3	0.43	2.4	20.0	43.0	26.0	44.0	19.0	42.0
7	7	7	7	0.42	2.4	17.0	37.0	22.0	39.0	16.0	37.0

TABLE II - continued

Conditions				Multichannel Image Devices[c,f]					
				4 Channels Illuminated with 4 Channels Measured[h]					
				0.0984 s Integration					
Device				V		SIT		ISIT	
Count Time, s[a]				1.05	32.8	1.05	32.8	1.05	32.8
log E_L	log E_B	log E_S	log[b] E_I						
5	3	3	3	0.008	0.05	1.9	10.0	3.4	19.0
5	3	3	7	0.008	0.04	0.35	1.3	0.48	1.4
5	3	7	3	0.008	0.04	0.35	1.3	0.48	1.4
5	3	7	7	0.007	0.04	0.24	0.72	0.33	0.77
5	7	3	3	0.008	0.04	0.29	0.48	0.36	0.49
5	7	3	7	0.007	0.04	0.22	0.45	0.29	0.47
5	7	7	3	0.007	0.04	0.22	0.45	0.29	0.47
5	7	7	7	0.007	0.04	0.19	0.40	0.24	0.41
7	3	3	3	0.78	4.4	49.0	210.0	70.0	260.0
7	3	3	7	0.74	4.1	28.0	92.0	39.0	100.0
7	3	7	3	0.74	4.1	28.0	92.0	39.0	100.0
7	3	7	7	0.70	3.9	22.0	59.0	29.0	63.0
7	7	3	3	0.74	4.1	25.0	47.0	32.0	48.0
7	7	3	7	0.70	3.9	20.0	43.0	26.0	44.0
7	7	7	3	0.70	3.9	20.0	43.0	26.0	44.0
7	7	7	7	0.67	3.7	17.0	37.0	23.0	39.0

TABLE II - continued

[a] 1.05 s corresponds to 32 machine cycles and 32.8 s to 1000 machine cycles at a cycle time of 32.8 ms.

[b] Photon irradiance units of photons s^{-1} cm^{-2}.
Flicker (fluctuation) factors $\xi_S = 0.003$; $\xi_B = 0.01$ for multichannel image devices and 0.00 for PM and ID.

[c] See Table I for detector efficiency and dark count rate used in calculations.

[d] Slit height 1 cm, slit width 0.01 cm.

[e] ID aperture of 10^{-4} cm^2.

[f] Devices assumed to be 1 cm high, 1.25 cm wide, and to contain 500 channels with lower half of each channel used for dark current subtraction. See g for SEC.

[g] Since the SEC has "no" dark current, the entire channel height is used for measurement of luminescence. Also, since the SEC is strictly an integrating device, it is read out only at the end of a measurement.

[h] 4 channels have the same width as the slitwidth used for the photomultiplier tubes (0.01 cm).

TABLE III
SIGNAL-TO-NOISE RATIOS FOR MOLECULAR LUMINESCENCE SPECTROMETRY

Conditions			Single Channel Devices[c]							
			Photomultiplier Tubes[d] with Photon Counting						Photon Counting	
Device			EMI 9558Q		EMI 6256S		ITT FW130		Image[e] Dissector	
Count Time, s[a]			1.05	32.8	1.05	32.8	1.05	32.8	1.05	32.8
$\log E_L$	$\log E_S$	$\log E_I$[b]								
4	2	2	1.4	8.1	10.0	56.0	14.0	75.0	0.32	1.8
4	2	6	0.75	1.6	0.87	1.6	0.87	1.6	0.03	0.18
4	6	2	0.75	1.6	0.87	1.6	0.87	1.6	0.03	0.18
4	6	6	0.51	0.81	0.55	0.81	0.55	0.81	0.02	0.13
6	2	2	98.0	290.0	130.0	310.0	130.0	310.0	4.6	25.0
6	2	6	61.0	110.0	67.0	110.0	67.0	110.0	2.6	15.0
6	6	2	61.0	110.0	67.0	110.0	67.0	110.0	2.6	15.0
6	6	6	44.0	65.0	46.0	66.0	46.0	66.0	2.0	11.0

[a] 1.05 s corresponds to 32 cycles and 32.8 s is 1000 cycles at the standard cycle time of 32.8 ms.

[b] Photon irradiance, units of photons s^{-1} cm^{-2}.
Flicker (fluctuation) factor $\xi_S = 0.003$.

[c] See Table I for detector efficiency and dark count rate used in calculations.

TABLE III - continued

Conditions			Multichannel Image Devices[c,f]							
			40 Channels Illuminated with 1 Channel Measured							
			No Integration							
Device			V		SIT		ISIT		SEC[g]	
Count Time, s[a]			1.05	32.8	1.05	32.8	1.05	32.8	1.05	32.8
log E_L	log E_S	log[b] E_I								
4	2	2	0.0002	0.001	0.06	0.31	0.11	0.62	0.33	3.7
4	2	6	0.0002	0.001	0.04	0.22	0.07	0.36	0.05	0.28
4	6	2	0.0002	0.001	0.04	0.22	0.07	0.36	0.05	0.28
4	6	6	0.0002	0.001	0.03	0.18	0.05	0.27	0.04	0.20
6	2	2	0.02	0.12	4.6	26.0	8.0	44.0	7.1	40.0
6	2	6	0.02	0.12	3.6	20.0	5.7	31.0	4.2	23.0
6	6	2	0.02	0.12	3.6	20.0	5.7	31.0	4.2	23.0
6	6	6	0.02	0.11	3.0	16.0	4.6	24.0	3.2	17.0

[d] Slit height 1 cm, slit width 0.1 cm.

[e] ID aperture of 10^{-4} cm^2.

[f] Devices assumed to be 1.0 cm high, 1.25 cm wide, and to contain 500 channels with the lower half of each channel used for dark current subtraction. See g for SEC.

TABLE III - continued

Conditions			Multichannel Image Devices[c,f]					
			40 Channels Illuminated with 1 Channel Measured					
			0.0984 s Integration					
Device			V		SIT		ISIT	
Count Time, s[a]			1.05	32.8	1.05	32.8	1.05	32.8
$\log E_L$	$\log E_S$	$\log E_I$[b]						
4	2	2	0.0004	0.002	0.10	0.56	0.20	1.1
4	2	6	0.0004	0.002	0.05	0.27	0.07	0.41
4	6	2	0.0004	0.002	0.05	0.27	0.07	0.41
4	6	6	0.0004	0.002	0.04	0.20	0.05	0.29
6	2	2	0.04	0.22	6.3	35.0	9.9	55.0
6	2	6	0.04	0.22	4.2	23.0	6.3	33.0
6	6	2	0.04	0.22	4.2	23.0	6.3	33.0
6	6	6	0.04	0.22	3.4	18.0	5.0	26.0

[g] Since the SEC has "no" dark current, the entire channel height is used for measurement of luminescence. Also, since the SEC is strictly an integrating device, it is read out only at the end of a measurement.

[h] 40 channels have the same width as the slit width used for the photomultiplier tubes (0.01 cm).

TABLE III - continued

Condition			Multichannel Image Devices[c,f]							
			40 Channels Illuminated with 40 Channels Measured[h]							
			No Integration							
Device			V		SIT		ISIT		SEC[g]	
Count Time, s[a]			1.05	32.8	1.05	32.8	1.05	32.8	1.05	32.8
$\log E_L$	$\log E_S$	$\log E_I$[b]								
4	2	2	0.001	0.008	0.35	2.0	0.70	3.9	2.1	24.0
4	2	6	0.001	0.008	0.25	1.1	0.40	1.3	0.31	1.2
4	6	2	0.001	0.008	0.25	1.1	0.40	1.3	0.31	1.2
4	6	6	0.001	0.008	0.20	0.68	0.30	0.75	0.22	0.70
6	2	2	0.14	0.79	29.0	150.0	50.0	220.0	45.0	200.0
6	2	6	0.14	0.79	22.0	84.0	34.0	97.0	26.0	89.0
6	6	2	0.14	0.79	22.0	84.0	34.0	97.0	26.0	89.0
6	6	6	0.14	0.78	18.0	57.0	27.0	62.0	20.0	58.0

TABLE III - continued

Condition			Multichannel Image Devices[c,f]					
			40 Channels Illuminated with 40 Channels Measured[h]					
			0.0984 s Integration					
Device			V		SIT		ISIT	
Count Time, s[a]			1.05	32.8	1.05	32.8	1.05	32.8
log E_L	log E_S	log[b] E_I						
4	2	2	0.003	0.01	0.63	3.5	1.3	7.0
4	2	6	0.003	0.01	0.31	1.2	0.46	1.4
4	6	2	0.003	0.01	0.31	1.2	0.46	1.4
4	6	6	0.003	0.01	0.23	0.70	0.32	0.76
6	2	2	0.25	1.4	40.0	190.0	62.0	240.0
6	2	6	0.25	1.4	26.0	89.0	37.0	99.0
6	6	2	0.25	1.4	26.0	89.0	37.0	99.0
6	6	6	0.25	1.4	21.0	58.0	28.0	62.0

consecutive readouts of a given channel is 32.8 ms).

(ii) If detector shot noise, preamplifier noise, photon shot noise, or any combination of these noises is the limiting noise, then the summation of signals and noises over n_c channels of an integrating image device (V, SIT, ISIT, or SEC) will improve the S/N by a factor of $\sqrt{n_c}$, assuming the signal and noise are constant over n_c channels.

(iii) Assuming that the PM is photon shot noise limited (i.e., a 1.05 s observation time), and that signal and noise are measured in one channel of the image device, then the S/Ns decrease in the following order:

PM > ISIT $\gtrsim$ SIT, SEC $\gtrsim$ ID >> V

(iv) Assuming photon (shot or flicker) noise limitation, with an observation time of either 1.05 s or 32.8 s, and the signal and noise for the image devices being summed over n_c channels, the S/Ns decrease in the following order:

PM $\gtrsim$ ISIT $\gtrsim$ SEC, SIT $\gtrsim$ ID >> V

(v) If source related flicker noises (interferences, scatter, or luminescence of analyte) are dominant, then the S/N of image devices vs. PMs will not improve with integration, summation over channels, or longer observation time.

(vi) The silicon vidicon, V, device is not analytically useful for atomic fluorescence or molecular luminescence spectrometry. Cooling would reduce the dark current and enable longer target integration times to reduce the preamplifier noise contribution which would result, in principle, in a much improved S/N. This improvement of course comes at the expense

of longer analysis time and the accompanying problems with long term noise (drift). A cooled vidicon has great potential for measuring weak sources as in astronomy, but is predicted to be of little or no analytical use. Experimentally, the vidicon has been shown to have little analytical use as a detector in atomic fluorescence flame spectrometry.[18]

(vii) The image dissector, ID, has a small format and small aperture requiring a spectrometer of small format, "high" resolution, and high luminosity (throughput) such as an echelle. For conventional unidirectional (not crossed) dispersion spectrometers, the ID is much less attractive (smaller S/N) than the PM even though the ID can slew scan at a much higher rate than conventional spectrometers. For a complex spectrum requiring high resolution and many spectral measurements (many resolution elements), the ID with an echelle spectrometer becomes more attractive compared to the PM or to the integrating type image devices (SIT, ISIT, and V); however, for such situations the SEC would appear to be the most generally useful detector.[9-11,59,60]

(viii) The linear dynamic range of the PM exceeds that of all the image devices because of its high sensitivity which results in a lower limit of detection and its immunity to target saturation which results in a higher upper limit compared to the SIT, ISIT, and SEC.[51,61] The ID has a linear dynamic range less than that of the photomultiplier, but greater than that of the integrating image devices.

(ix) Image devices, except for the ID, are plagued with

background noise problems (i.e., radiation not connected with the source), particularly in atomic fluorescence flame spectrometry. Synchronous operation would reduce it, but would not be highly efficient due to the limited repetition rate imposed by the scan time of integrating image devices.

(x) The photon irradiance (photons cm^{-2} s^{-1}) necessary for a detector to become photon noise limited (shot or flicker) is lower for more sensitive detectors, is greater for photon flicker than photon shot noise and is greater in atomic than molecular luminescence spectrometry (due to the larger slit widths typically used in molecular luminescence spectrometry).

(xi) It should be stressed that all of the S/N results for the PM cases given in this manuscript are concerned with the measurement of a single spectral interval. If m spectral intervals are measured via a sequential linear scan spectrometer (SLS) or r ($m \geq r$) spectral components are measured via a sequential slew scan spectrometer (SSS) during a given measurement time t_o, the S/N for any given spectral interval (channel) will necessarily decrease (or at best not change). The effect of the optical measurement systems upon S/N has already been discussed by Winefordner et al.[54]

Specific Conclusions Regarding Atomic Fluorescence Spectrometry

(i) Assuming source related photon shot noise for the PM (1.05 s observation time), if one channel is measured for the integrating image devices, then the S/N decrease in the following order:

PM > ISIT ≳ SIT, SEC > ID >> V

If four channels of the integrating image devices are summed, or if an observation time of 32.8 s is used (in which case the PM becomes primarily flicker noise limited), the PM and ISIT are within a factor of 2. The FW 130 PM is always as good as or better than the 6256S PM, which is always as good as or better than the 9558Q PM.

(ii) Assuming detector-preamplifier noise limitation and an observation time of 32.8 s for the image devices, and an observation time of 1.05 s for the PM, and summing over four channels with three integrations between scans, the S/Ns decrease in the following order:

SEC ≳ ISIT ≳ SIT ≳ PM ≳ ID >> V

The FW 130 PM and 6256S PM give S/N at 1.05 s similar to the SIT at 32.8 s, but the 9558Q PM at 1.05 s gives a much poorer S/N than the SIT, ISIT, and SEC.

(iii) Assuming background noise limitation ($E_{pL} \leq 10^{-2}$ E_{pB}, e.g., $E_{pL} = 10^{5}$ and $E_{pB} = 10^{7}$ photons s^{-1} cm^{-2}), if either a 1.05 s or a 32.8 s observation time is used, then the S/Ns decrease in the following order:

PM > ISIT ≳ SEC, SIT ≳ ID >> V

If four channels of the image devices are summed for a 1.05 s observation time, the S/N for the PM and ISIT are within a factor of 2. The S/N of the three PMs are identical for a 32.8 s observation time, however for 1.05 s the FW 130 ≳ 6256S ≳ 9558Q.

(iv) (a) The maximum number of resolution elements re-

quired for the measurement of complex atomic spectra as in atomic emission spectrometry of high temperature plasmas is approximately 6×10^4 (800 - 200 nm divided by the spectral bandwidth or line width, $\delta\lambda \sim 0.01$ nm). The maximum number of resolution elements required for the measurement of complex atomic absorption spectra (AAS) or atomic fluorescence spectra (AFS) is approximately 6×10^3 (i.e., the value of $\delta\lambda$ can increase to 0.1 nm with AAS and AFS and still not have significant spectral overlap in most cases).

(b) Because the number of effective channels of V, SIT, and ISIT is ~ 200 (500 actual channels, but spreading of the images results in a loss here, one channel is taken to spread into "on the average" 2.5 channels), the number of spectral windows needed to cover 200 - 800 nm in AES is ~300 and in AAS, AFS, or flame AES is ~30 assuming all windows contain sufficient spectral information to warrant measurement.[1,2,41] Although the AES high temperature plasma case is hardly a tenable one, the AAS, AFS, and flame AES cases appear to be potentially useful. However, such an image device system must be weighed against a direct reading multichannel system as well as a slewed scan single channel PM case. Finally, the usefulness of the image device may increase in AAS, because the windows can be increased considerably with the concomitant loss in S/N assuming appropriate line sources with simple spectral outputs are available.

(c) For the case where a large number (say 10 - 100) of spectral lines in a complex spectrum, e.g., emission

spectrum from a high temperature (>4000 K) plasma, must be resolved and measured, an echelle spectrometer with the SEC is a more analytically useful detector because the number of channels is greatly increased (>2000).[11,59,60]

(d) For the case where a smaller number of spectral lines (≈10) in a complex spectrum must be resolved and measured, an echelle spectrometer with ID would be an analytically useful system. Because of the rapid slew rate of the ID, the additional use for observing rapid transients is also possible.[9,10]

(e) For the case where a predetermined large number (10 - 50) of spectral lines in a complex spectrum must be resolved and measured, a multichannel direct reader is certainly optimal, whereas for the measurement of a smaller number (≈10) of predetermined spectral lines in a less complex spectrum a slewed scan single channel spectrometer with PM is optimal.[54]

(v) The S/N of image devices requiring scintillators to enhance their UV response is even lower compared to PM because even though in both detectors the photocathode efficiency varies with wavelength, with scintillators there is an additional conversion efficiency which is less than unity, e.g., ≈0.1.[61] The lower sensitivity of image devices as the SIT, and ISIT (with scintillators) in the UV region requires longer measurement times to achieve adequate S/N and thus there is only a small range of signals where photon shot noise is limiting in AFS.

Specific Conclusions Regarding Molecular Luminescence Spectrometry

(i) Assuming photon noise limitation (shot or flicker), if either a 1.05 s or a 32.8 s observation time is used, and forty channels are summed for the integrating image devices, then the S/N decrease in the following order:

PM $\gtrsim$ ISIT $\gtrsim$ SIT, SEC > ID >> V

(ii) Assuming photon noise limitation (shot or flicker), if only one channel of the image device is measured, then for a 1.05 s or 32.8 s observation time, the S/N of the integrating image devices become several times poorer than the S/N of the PM.

(iii) Assuming preamplifier noise limitation, if a 32.8 s observation time is used, and there is summation over forty channels of the integrating image device, then the S/N decrease in the following order:

PM > SEC > ISIT $\gtrsim$ SIT $\gtrsim$ ID >> V

(iv) Because the S/N of image devices (ISIT, SIT, and SEC) are close to the S/N of PM for the case of photon (shot or flicker) noise limitation (which is common in analytical luminescence spectrometry) these image devices possess a time advantage since they record many spectral components simultaneously (multichannel advantage). With regards to quantitative analysis, similar detection limits should be achieved with the SIT, ISIT, SEC, or PM. VoDinh et al., have obtained similar detection limits for several organic molecules by conventional spectrofluorimetry using either an SIT or PM detector (PM about 5 fold better).[35]

(v) The integrating image devices (ISIT, SIT, SEC, and V for high incident light photon fluxes) have considerable analytical potential. They perform adequately compared with a PM when measuring steady state molecular luminescence or absorption. In addition, they function particularly well when measuring transient molecular luminescence or absorption, e.g., when acting as a detector for liquid or gas chromatography. Rapid scan spectrometers with PM or ID would be expected to and generally have resulted in reduced S/N ratios for the large wavelength regions scanned in molecular luminescence (absorption) spectrometry. In comparison, the integrating image detectors are capable of giving more spectral information, with greater spectral fidelity and little loss in S/N ratio as compared to single channel measurements with a PM system.

Gas Phase Fluorescence Detection with the SIT

"Real Time" Mode

One of the main features of the SIT is the capability to detect and display instantaneously a temporally changing signal (over a wide spectral region), thus making this device quite suitable for chromatographic techniques. The experimenter can therefore observe the whole spectra of various compounds under study as they pass through the flow cell, making possible a rapid, semiqualitative identification. The real time signal from any of the 500 channels is also fed into a strip chart

recorder to give a conventional fluorescence chromatogram which is similar to that obtained with a single channel detector (e.g., photomultiplier). However, in this mode, the SIT has a 50 - 100 times poorer sensitivity than the photomultiplier. Therefore, for quantitative analysis, the integration mode of the SIT, which will be discussed in the next section, is preferred. The real time mode is illustrated in Figures 5A and 5B.

Integration Mode

In the integration mode, the SIT/OMA system accumulates data over a designated time period. The final recorded spectrum consists of the total integrated signals of each of the 500 channels accumulated over the entire observation time. These principles are illustrated in Figures 5A and 5C. Data accumulation leads to a significant improvement in the signal-to-noise ratio as discussed below. The linearity of the SIT response vs. measurement time has been previously investigated and is known to be quite suitable for chromatographic detection.[48] There are two practical factors which limit the integration time of an SIT; the dynamic range is limited by overflow of the memory ($\sim 10^5$ counts) and the chromatographic peak width is limited. Data accumulation times longer than the chromatographic width will not lead to any signal-to-noise enhancement. Figures 6 and 7 show the data integration results in two typical cases: in Figure 6, for a chromatographic peak halfwidth of 18 s, integration times up to 12.8 s provide a

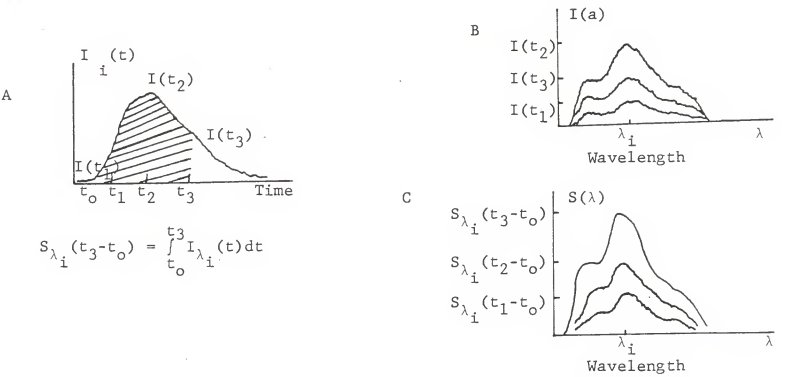

Figure 5. Various Operating Modes of the SIT/OMA.

A. The change in sample concentration (or fluorescence intensity) observed at one wavelength λ_i.

B. Real time mode display by the OMA of the entire spectrum, observed at times t_1, t_2, and t_3.

C. Multichannel display of the entire spectrum after data accumulation over a time period between t_1 and t_o, t_2 and t_o, and t_3 and t_o.

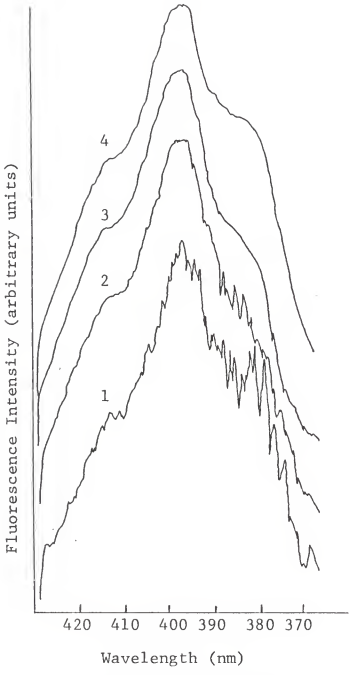

Figure 6. Dependence of Signal-to-Noise Ratio on Chromatographic Peak Width and Integration Time. For a Peak Halfwidth of 18 s.

Data taken over 12 (curve 1), 50 (curve 2), 200 (curve 3), and 800 (curve 4) accumulation cycles. The peak heights of each spectrum are normalized to the same value.

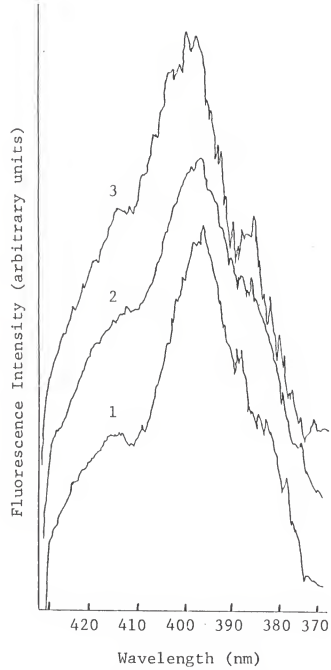

Figure 7. Dependence of Signal-to-Noise Ratio on Chromatographic Peak Width and Integration Time. For a Peak Halfwidth of 2 s.

Data taken over 12 (curve 1), 50 (curve 2), and 200 (curve 3) accumulation cycles. The peak heights of each spectrum were normalized to the same value.

significant signal-to-noise improvement. On the other hand, in Figure 7 where the chromatographic halfwidth is only 2 s, an accumulation time of 6.4 s does not provide any increase in signal-to-noise ratio over an accumulation time of 2 s.

Background Correction

Background correction was accomplished by use of the A - B mode, as described in the experimental section. Luminescence background from the solvent or carrier gas impurities could be corrected by recording into memory B the signal, if any, generated by injecting a solvent blank. Because scattered light has been found to give a significant contribution to the observed signal, this correction procedure was most important. At the same time, all other undesired interferences, such as quartz cell emission and dark signal from the detector, were also eliminated.

Spectral Selectivity and Mixture Analysis

As has been pointed out by previous authors, the combination of fluorescence and chromatography provides a powerful tool for the analysis of mixtures containing fluorescent compounds.[42-46] Due to its inherent sensitivity, the fluorescence system is able to detect many compounds at the nanogram or sub-nanogram level. Since non-fluorescing compounds do not generate a signal, they do not interfere with an analysis as they might with a more universal detector. Fluorescent compounds themselves can be resolved chromatographically and/or

spectroscopically. For example, two or more fluorescent compounds which fluorescence spectrometry alone might not be able to differentiate in a mixture can often be separated in time or space (i.e., chromatographically) so that the detector can examine each compound separately. Alternatively, compounds which are not separated chromatographically may be discriminated from one another and identified by means of their characteristic fluorescence excitation and/or emission spectra.

The use of the SIT/OMA system enhances the spectral selectivity of vapor phase fluorescence detection. Even though simultaneously eluting compounds with overlapping emission spectra can perhaps be partially resolved by the selective excitation of one of the compounds, complete resolution may not always be possible. In this case, the ability of the OMA to subtract stored signals from one another can be used to obtain the desired information. An illustration of this capability is shown in Figure 8. Curve 1 in Figure 8 represents the combined emission signals from a mixture of anthracene and benzo-[a]-pyrene. When the signal obtained from an injection of pure anthracene (same amount in both cases) is subtracted from curve 1, the spectrum of benzo-[a]-pyrene (curve 3) is obtained. Similarly, the spectrum of anthracene (curve 2) is obtained when the signal from an injection of pure benzo-[a]-pyrene (same amount in both cases) is subtracted from curve 1.

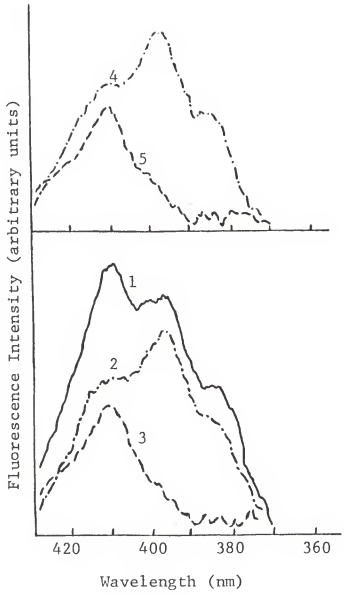

Figure 8. Gas Phase Fluorescence Spectrum of a Mixture of Anthracene and Benzo-[a]-pyrene.

1. Original spectrum of the mixture
2. After subtraction of the benzo-[a]-pyrene spectrum
3. After subtraction of the anthracene spectrum
4. Spectrum of pure anthracene
5. Spectrum of pure benzo-[a]-pyrene

Gas Phase Luminescence Spectra

The gas phase luminescence spectra observed in the experiments at gas chromatographic temperatures illustrate a few typical features which deserve comment. In Figure 9, two gas phase (curves 1 and 2) and one condensed phase (curve 3) spectra of anthracene obtained with the SIT system are shown (5 nm spectral band pass). The dependence of the shape of the gas phase spectrum upon excitation wavelength is evident, with the spectrum resulting from the 0 - 0 band excitation (346 nm) bearing a closer resemblance to the condensed phase spectrum. The typical blue shift (about 5 nm) which occurs when going from the condensed to gas phase fluorescence is also shown, along with a general blurring of the spectrum. At the elevated temperatures needed to separate high boiling polyaromatic hydrocarbons by gas chromatography, the free vibrational molecular motions and Doppler and collisional broadening processes are believed to contribute to the diffuseness of the vapor phase luminescence spectra. As shown in curve 2 (Figure 9), increase in the energy of excitation (246 nm) gives rise to a red shift along with a change of the intensity distribution in the vapor phase fluorescence spectrum. These results are in agreement with data reported by previous workers.[48,62] From these considerations, it is seen that great care must be taken to perform quantitative analysis at constant temperature and specified excitation energy.

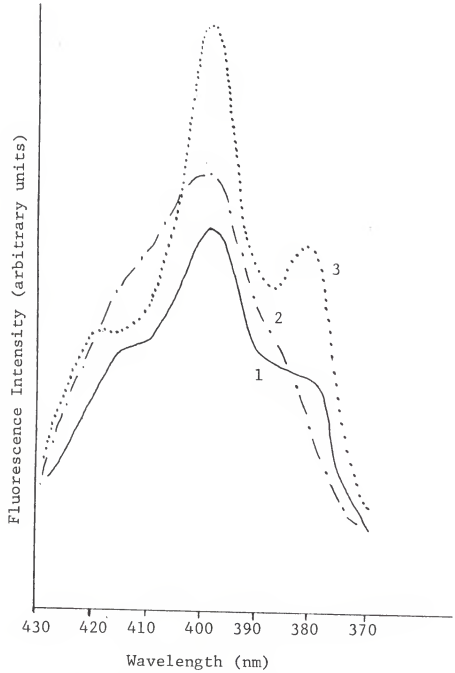

Figure 9. Fluorescence Spectra of Anthracene.

1. Gas phase, λ_{exc} = 347 nm
2. Gas phase, λ_{exc} = 246 nm
3. Condensed phase, λ_{exc} = 246 nm

Limits of Detection and Analytical Curves

The analytical curve for anthracene is given in Figure 10, and the detection limits of several polyaromatic hydrocarbon molecules are shown in Table IV. Peak heights at the peak fluorescence wavelength in the accumulated spectrum are used as a measure of luminescence intensity. The experimental gas chromatographic temperature is 265°C for benzo-[a]-pyrene and 200°C for all other compounds. The data accumulation time is 6.4 s for most compounds, except for pyrene (9.6 s). Typical limits of detection are reported together with the corresponding values obtained with a photomultiplier tube. Detection limits with the SIT, although 3 - 5 times larger than those obtained with the photomultiplier, are particularly low and are all at the nanogram level.

At or near the limit of detection, the limiting noise is equivalent to the noise on the baseline observed on the A - B display, where both memories have accumulated background for the same period of time. When measuring either dark counts or background scatter from the xenon lamp, the signal-to-noise ratio improves by a factor of about 1.75 when the amount of accumulation time is increased by a factor of 4. This nearly square root dependence indicates that the noise is predominantly shot noise, and that a further improvement in the limit of detection could be obtained by increasing the light throughput of the system.

Another characteristic of the SIT is a coherent sinusoidal noise pattern (possibly 120 Hz) which is observable on the real

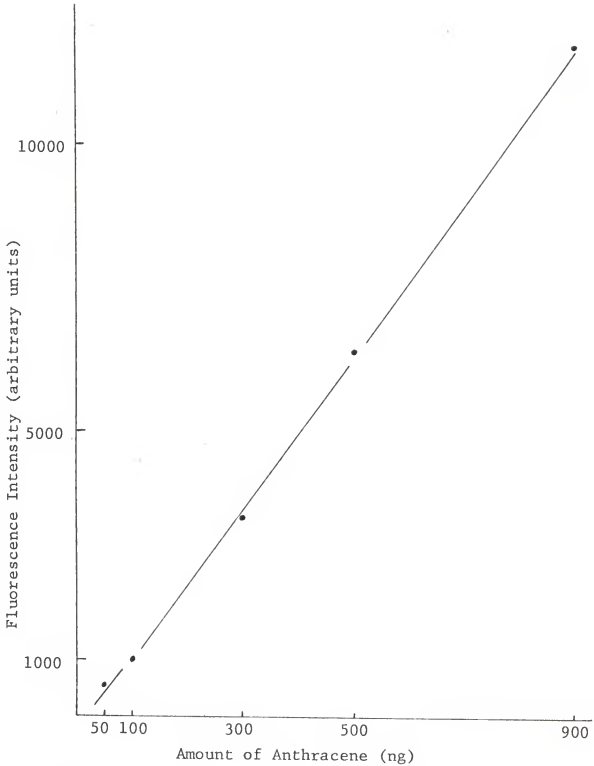

Figure 10. Analytical Curve of Anthracene in the Gas Phase Obtained with the SIT.

TABLE IV
LIMITS OF DETECTION OF SEVERAL POLYAROMATIC HYDROCARBONS BY AN SIT IMAGE VIDICON FLUORESCENCE DETECTOR GAS CHROMATOGRAPHIC SYSTEM

Compound	λ_{exc} [nm]	λ_{em} [nm]	Temp. °C	Integration Time [s]	L.O.D.[a] SIT[b] [ng]	L.O.D.[a] PM[c] [ng]
Anthracene	(266)	400	200	6.4	1.0	0.20
Pyrene	(316)	360	200	9.6	1.5	0.23
Phenanthrene	(256)	375	200	6.4	2.5	0.51
Chrysene	(265)	400	200	6.4	15.0	2.0
Benzo-[a]-pyrene	(281)	430	265	6.4	6.5	-

[a] Limit of detection is that amount of analyte, in ng, resulting in a S/N = 3 (N = rms noise).

[b] SIT = silicon intensified target detector, spectral bandwidth of 5 nm, observation time of 6.4 s for all compounds except pyrene (9.6 s).

[c] PM = photomultiplier detector, spectral bandwidth of 25 nm, observation time of 1 s, operated in non-scanning mode.

time display and is carried through to the A (or B) memory display(s) in the accumulation mode. This pattern may or may not show up in the A - B mode depending upon whether or not the pattern in memory B is in or out of phase with that in memory A. The relative magnitude of this effect is inversely proportional to the number of accumulation cycles. The coherent noise can therefore diminish the signal-to-noise ratio by a significant factor, e.g., 2 or 3, if the light flux to the detector is small. It should be stressed here that grounding of the measurement system is very important to minimize the coherent noise.

When used as detectors for liquid or gas chromatography, both fast scanning (single channel) and SIT (multichannel) systems are measuring transient signals, the intensities of which vary as the compound of interest passes through the detector.[63] The actual period of time (t_o) that either system spends observing the analyte signal is limited to an optimal value of t_w, the peak width of the eluting substance.

A fast scanning system looks sequentially at a total number, N, of spectral intervals, $\Delta\lambda$ (where $\Delta\lambda$ is determined by the spectral bandpass of the spectrometer). The total wavelength region covered by a scan is $N\Delta\lambda$. The actual time spent observing each individual spectral interval ($\Delta\lambda_i$) would be $(1/N)t_o$, while the rest of the time, $(N - 1/N)t_o$, would be spent examining the remaining N - 1 spectral intervals.

As mentioned earlier, the SIT partitions a spectral region of interest into 500 spectral components, or channels.

Each channel is "on", accumulating data, over 99.9% of the time, being "off" only momentarily once every 32.8 ms while its data are being stored in memory. Thus assuming equivalent resolution, observation time, and total spectral region covered, the SIT will collect 0.999/(1/N) or about N times as much information as the fast scanning system. It should be noted that due to the limitations of both systems (discussed below), the assumed conditions will rarely, if ever, be met in practice.

Due to the sequential nature of the fast scanning system, there is an unavoidable lag between the time the ith spectral interval is observed and the time the jth spectral interval is observed. During this time lag ($\{[j - i]/N\}t_o$), there will be a change of analyte concentrate in the detector cell causing a change in overall signal intensity, which may result in a distortion of the observed spectrum. The distortion becomes worse for lower scan rates and/or a larger spectral region to be covered and/or a greater mass flow rate through the detector. The problem of distortion can be counteracted somewhat by increasing the scan rate, so that the relative intensities of the individual spectral intervals vary little throughout the duration of the scan. Increasing the scan rate however decreases the observation time, t_o, thus wasting useful information. In addition, after the scan rate is increased past a certain point, resolution deteriorates (even if special readout equipment is used, resolution still may degrade).

As discussed earlier, each of the SITs spectral channels

obtains information simultaneously, in parallel. As a result, not only is analyte signal observed for the entire peak width, t_w, but also there is little spectral distortion due to the transient nature of the signal, assuming the chromatographic peak width is significantly greater than 32.8 ms.

There is no provision for background correction in a fast scanning system. If the background is not constant over the wavelength region scanned, then the observed spectrum will be distorted. As pointed out in the experimental section, background variation is accounted for with the SIT detector. However, both the SIT and the PM have the disadvantage of variation of sensitivity (spectral) with wavelength; the SIT in addition has a response which varies with channel number (spatial). The fast scanning system has the distinct advantage of being able to recover both excitation and emission spectra, while the SIT is limited to emission spectra only.

The SIT system used in this study can at any one time examine a total spectral region of only about 60 nm. Because no one 60 nm region encompasses the emission spectra of all possible fluorescent compounds of interest, this is a drawback of this SIT system. Indeed, the emission spectra of some compounds are themselves more than 60 nm wide. This problem could be overcome by decreasing the spectral dispersion of the spectrometer (with concomitant loss of resolution) or alternatively by a progression in vidicon technology providing a larger active surface on the face of the TV tube. A fast scanning system possesses the ability to scan the

entire wavelength region from 200 to 800 nm. However, as discussed earlier, scanning larger wavelength regions results in problems of spectrum distortion and decreased observation time for each spectral interval scanned.

Condensed Phase Fluorescence Detection with the SIT

In Table V, limits of detection are given for several polynuclear aromatic and heterocyclic compounds of biological interest using the simulated liquid chromatograph with SIT detector discussed above. Here, the limit of detection is defined as the absolute amount (ng) of material injected which gives a S/N_{rms} equal to 3. Heights of the most intense spectral bands were used as the measure of luminescence intensity, while the rms noise was 0.2 times the peak-to-peak baseline noise, as discussed in the section on theoretical considerations. All compounds but one were detected in the subnanogram range. Thus, considering its good sensitivity and multichannel advantage there is obviously great potential use for the SIT and similar devices as detectors for liquid chromatography, even more so than for gas chromatography, where the spectra are less detailed than they are in solution.

In Figure 11, log-log plots are given of signal (curves S_1, S_2, and S_3) and noise (N_1, N_2, and N_3) vs. time for steady state fluorescence emission of intensities of 38, 280, and 575 counts per accumulation cycle, respectively.

Curves S_1, S_2, and S_3 all have slopes of unity, demon-

TABLE V
LIMITS OF DETECTION OF SEVERAL POLYAROMATIC AND HETEROCYCLIC MOLECULES

Compound	Solvent	Carrier Solution	λ_{exc}[a] [nm]	λ_{em}[a] [nm]	Δt[a] [s]	ΔT[a] [s]	L.O.D.[a] [ng]
Perylene	Hexane	Methanol	410	468	25	32.8	3.0×10^{-2}
Anthracene	Hexane	Methanol	250	403	25	32.8	2.0×10^{-2}
Chrysene	Hexane	Methanol	280	380	25	32.8	8.0×10^{-2}
Benzo- a -pyrene	Hexane	Methanol	350	440	25	32.0	1.5×10^{-1}
Riboflavin	Water:Methanol (5/100; V/V)	Water	430	523	25	37.8	6.5×10^{-1}
Acridine	Methanol	Water	346	419	25	37.8	2.3×10^{-1}
4,5-Diphenyl-imidazole	Methanol	Water	285	390	25	32.8	4.5

[a] λ_{exc}, λ_{em} = excitation and emission wavelengths giving maximum fluorescence intensity.
Δt = delay time between injection and measurement.
ΔT = measurement time (1000 accumulation cycles).

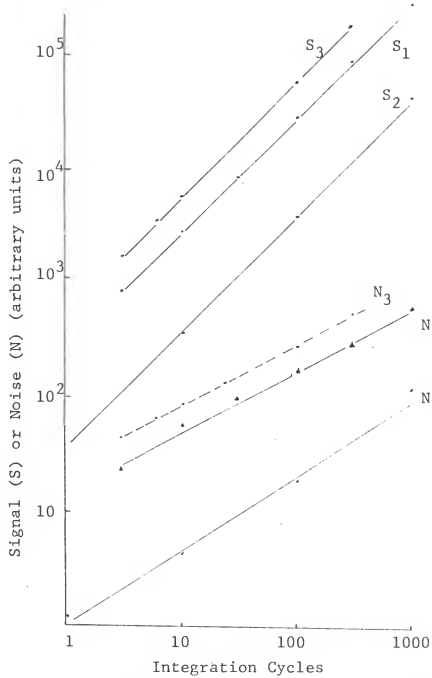

Figure 11. Plots of Signal (S_1, S_2, S_3) and Noise (N_1, N_2, N_3) vs. Number of Accumulation Cycles at Different Count Rates.

S_1 and N_1 taken at 280 counts cycle^{-1}, S_2 and N_2 taken at 38 counts cycle^{-1}, S_3 and N_3 taken at 575 counts cycle^{-1}. Curves S_1, S_2, and S_3 have slopes of 1, curves N_1 and N_3 have slopes of 0.5, curve N_2 has a slope of $\sim$0.6.

strating that the response of the SIT is linear with signal intensity over the range studied, which is what was expected, because the stated range of linearity of the OMA is close to 780 counts per accumulation cycle. For the two highest count rates, log-log plots of noise vs. observation time (N_2, N_3) have slopes of 0.5, showing that at relatively high signal levels, shot noise (either photon or detector) predominates. Because the highest count rate observed is very close to the saturation rate (780 counts per accumulation cycle), it may be that for this system, photon flicker noise will never become dominant. The noise vs. observation time plot for the lowest count (N_1) rate has a slope of 0.6, indicating that some type of noise, in addition to shot noise, is present. Because it is present at low signal levels, it cannot be source related flicker noise, and detector electronics flicker noise is assumed to be negligible. It seems likely that the additional noise is a coherent pattern noise observed previously in the author's laboratory. However, this noise has not been fully characterized, so it is not possible to say what the exact time dependency of this type of noise is, other than as the observation time increases, photon or detector shot noise eventually becomes dominant.

Comparison of SIT and SLS

Figures 12 and 13 show spectra obtained from a 4×10^{-4} ppm anthracene solution using the SIT and SLS systems, respectively.

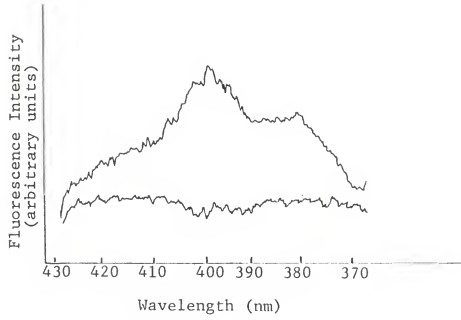

Figure 12. Spectrum of Anthracene (10^{-4} ppm) in Methanol Obtained with the SIT (Observation Time = 32.8 s). Spectral Bandpass = 10 nm. Bottom Curve is Spectrum of Methanol Blank.

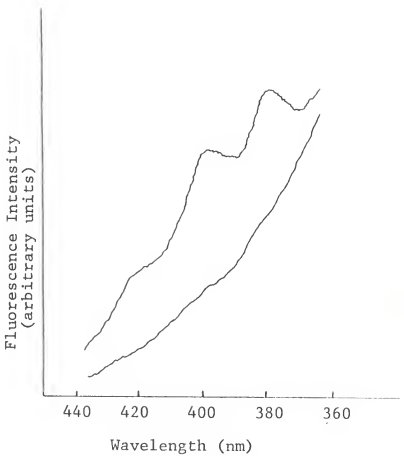

Figure 13. Spectrum of Anthracene (10^{-4} ppm) in Methanol Obtained with the Photomultiplier Tube (1P21, System Response Time = 2.3 s, Scan Rate = 1.9 nm s^{-1}). Spectral Bandpass = 10 nm. Bottom Curve is Spectrum of Methanol Blank.

Both spectra in Figure 12 were obtained using the A - B display mode of the OMA. In the upper spectrum, sample emission was contained in memory A and blank emission was in memory B, while in the baseline (lower spectrum) blank emission was in both memories. In Figure 13, the solid line is the sample spectrum while the dashed line shows the blank spectrum.

The limits of detection (for $S/N_{rms} = 3$) calculated from the spectra are 1.2×10^{-5} ppm for the SIT and 4.2×10^{-6} ppm for the SLS. Several points should be kept in mind concerning this comparison, however. The output signal from the PM is a current, or a charge flow. The current magnitude, or rate of charge flow is directly proportional to the rate at which photons strike the photocathode. Thus the basic information contained in the PM signal is rate information. Therefore, when the PM is not used as an integrating detector, its signal will be independent of the observation time, t_o, in the sense that for a constant photon flux, the PM signal will have constant magnitude, for however long the measurement is made. Due to the electrical bandwidth, Δf, of the system, the PM (SLS) signal does possess some time dependency. For example, it takes a finite time ($\approx \Delta f^{-1}$) to reach a steady state value, and it must also be remembered that the magnitude of the output signal at any time, t, actually depends upon the average input signal from time, $t - t_a$, to time t (where t_a is the averaging time of the system, $= 1/2\Delta f$).[64]

The SIT, on the other hand, is an integrating detector, therefore the output signal is in terms of total accumulated

charge, or counts. The magnitude of the output signal depends upon both the rate at which photons strike the detector and the total observation time, t_o, regardless of whether or not the rate of photon arrival at the detector is constant.

In the spectrum generated from the PM, the wavelength axis is also a time axis because as the spectrometer scans wavelength, the information for any given spectral interval is obtained at a time different from that in which information for all other spectral intervals is obtained.

In the spectrum generated from the SIT, the wavelength axis is <u>not</u> also a time axis, as in the case of the SLS, because the information accumulated in one spectral interval is accumulated simultaneously with the information in all other spectral intervals. Thus, spectra from the two systems, although having the same general appearance, will be different in that the PM spectrum plots current (rate) vs. wavelength (time) while the spectrum from the SIT plots counts (total accumulated charge) vs. wavelength.

The SLS system generates its printed spectrum at the same time it scans. The scan rate (R_s, nm s^{-1}) is limited to a range of values such that:

$$R_s \leq \frac{\delta\lambda_b}{t_r} \tag{10}$$

where $\delta\lambda_b$ is the halfwidth (in nm) of the narrowest spectral feature to be recorded, and t_r is the response time of the system, equal to $1/2\Delta f^{-1}$, Δf being the limiting, or smallest,

bandwidth of the entire system, including recorder.[64] As seen below, this can greatly affect the total analysis time of the PM system.

The SIT system generates a printed spectrum by sequentially reading the digital contents of each memory (A or B) location, or sequentially subtracting the digital contents of corresponding locations in both memories (A - B mode), and passing the desired information through a D-A converter to a chart recorder. Thus the spectrum actually is composed of 500 discrete points, and if the chart speed were fast enough compared to the OMA readout rate, the spectrum would consist of a series of steps. Usually, however, the chart speed is slow enough relative to the OMA readout rate that the spectrum has a "continuous" appearance. Also, if the readout time per channel of the OMA is shorter than the recorder response time, this will have the effect of "smoothing" out the spectrum, that is, both making the spectrum look more "continuous" and also damping out the noise fluctuations from channel to channel. Since the spectrum is printed subsequent to the actual observation, the time it takes to print the spectrum must be taken into account if the total analysis times of the two systems are to be compared. For the OMA used in this study, the printout time ranges from 16.4 s to 3.00 min in 16.4 s increments.

In the A - B mode, the SIT takes the sample spectrum (A memory) and subtracts the blank spectrum (B memory) to yield the "corrected" spectrum for a "complete" analytical determination (sample minus blank). This means that the A - B spec-

trum contains noise contributions from both the sample and the blank, as indicated in equation 5. In contrast, the SLS system prints either the sample or the blank spectrum, but it does not print a single spectrum containing sample minus blank information. Therefore (contrary to equation 9, which contains noise contributions from both sample and blank), a spectrum generated from the SLS system contains a noise contribution from either sample or blank, but not both. Thus a rigorous experimental comparison of the two systems requires that the noise measured on the PM spectrum be multiplied by a factor of between 2 and $\sqrt{2}$ depending upon whether the dominant noise is flicker or shot noise, respectively. It is not always convenient to determine the nature of the limiting noise, however, and failure to do so introduces at most an error of only $\sqrt{2}$ in the comparison.

Also, the bandwidth of the SIT ($\Delta f_{SIT} = 7.6 \times 10^{-3}$ Hz) is about 65 times smaller than that of the SLS ($\Delta f_{SLS} = 0.5$ Hz). Because shot noise is directly proportional to $\Delta f^{\frac{1}{2}}$, the S/N of the SLS would have improved by a factor of $\sqrt{65}$ or ≈ 8 if Δf_{PM} had been made equal to Δf_{SIT}, and therefore the limit of detection with the PM would have been lower by a factor of ~ 8 (assuming shot noise predominance).

In addition, the readout time of each memory channel of the OMA was ≈ 260 ms, while the response time of the recorder, t_r, was ≈ 460 ms, so the recorder will have smoothed out somewhat the noise inherent in the SIT spectrum. In the SLS case, the scan rate, R_s, was 1.9 nm s^{-1}, well below maximum usable

rate of

$$\frac{\delta\lambda_b}{t_r} = \frac{10 \text{ nm}}{4.6\text{x}0.5 \text{ s}} = 4.3 \text{ nm s}^{-1}$$

It is also interesting to compare the analysis time for both systems (disregarding sample preparation and handling, etc.). The analysis time for the SIT was about 3.5 min (about 0.5 min each for data accumulation into memory A and memory B, and a little over 2 min for spectrum printout). The analysis time for the SLS system was a little over 1 min (scanning ∿62 nm twice at 1.9 nm s^{-1}) and could have been even less if it had scanned at the maximum usable rate (4.3 nm s^{-1}). Thus, the SLS has a slight advantage over the SIT (in the measurement of steady state fluorescence) with regard to both lower limit of detection and faster analysis time.

However, if the SLS had had the same bandwidth as the SIT, as discussed above, its maximum usable scanning rate would have been

$$R_s = \frac{10 \text{ nm}}{158 \text{ s}}$$

or 0.063 nm s^{-1}, and the scanning time for a 62 nm spectral window would become over 16 min.

Thus it can be seen that there is a tradeoff between analysis time and limit of detection for both the SLS and SIT systems. For the SIT, increasing the signal-to-noise ratio by a factor of n requires increasing the accumulation time by a factor of n^2. For the SLS, increasing the S/N by a factor of

n requires decreasing the bandwidth and decreasing the scan rate by a factor of n^2.

This tradeoff between analysis time and limit of detection may or may not be important in the SLS system for the analysis of steady state signals, but it certainly must be considered when making measurements of transient signals such as those discussed earlier in this paper.

Instrumental Effects on S/N

Comparison Study

Table VI lists the limits of detection for four different polynuclear arenes using systems i, ii, and iii. In all cases but one, there is less than a factor of three difference between the highest and lowest limit of detection for a given compound. The limits of detection for the Eimac lamp in the pulsed mode are worse than the limits of detection for the same lamp run in the continuous (cw) mode. This results from a combination of several factors. First, the peak UV flux in the pulsed mode is greater than the average UV flux in the cw mode, whereas the peak visible flux in the pulsed mode and the average visible flux in the cw mode are about the same. Secondly, being a pulsed system, the average signal, background, and noise will also depend upon the duty factor of the system (in this case, the duty factor is about 6×10^{-3}).[55] All these factors taken together result in a net reduction in signal-to-noise ratio and increase in limit of detection.

TABLE VI
LIMITS OF DETECTION (in ng) FOR FOUR POLYNUCLEAR ARENES OF SYSTEMS i, ii, AND iii (SEE TEXT FOR DESCRIPTION), ALONG WITH EXCITATION AND EMISSION MAXIMA (in nm).

Compound	System i			System ii			System iii		
	LOD (ng)	λ_{ex} (nm)	λ_{em} (nm)	LOD (ng)	λ_{ex} (nm)	λ_{em} (nm)	LOD (ng)	λ_{ex} (nm)	λ_{em} (nm)
Pyrene	0.23	276	383	0.90	265	383	0.45	281	283
Anthracene	0.20	246	398	0.48	246	398	0.18	256	398
Chrysene	2.0	266	376	3.5	266	376	2.0	276	376
Phenanthrene	0.51	256	366	1.3	256	366	0.66	261	366

The similarity of the limits of detection of systems i and iii results from compensating differences in the two systems. The mercury-xenon arc lamp is somewhat more intense than a xenon arc lamp, while the Eimac xenon lamp collects a greater solid angle than do the ellipsoidal optics of the Aminco system. These two properties must effectively cancel out, making the limits of detection virtually identical.

Table VII lists the limits of detection for anthracene obtained with several different systems, of which i, ii, and iii have already been discussed. System iv gave some slight improvement over the first three. However, in this case, the high intensity of the laser source was offset to some extent by the fact that the 337 nm exciting wavelength is not the most efficient for anthracene or other polynuclear arenes. Also, it is not known whether the pulse to pulse stability of the laser source had an adverse effect on the S/N.

The better (smaller) limit of detection for system v may be due to the fact that the excitation monochromator employed was blazed within 5 nm of the excitation maximum of anthracene. Also, the overall efficiency of the system may have been greater and the amount of the stray light less than that of the other systems.

It should be noted that the flow cell temperature in systems iv and v was lower than in systems i, ii, and iii. However, while it has been shown that the sensitivity of gas phase fluorescence detection increases at lower temperatures, in this case, the temperature differential was not enough to make a

TABLE VII
LIMITS OF DETECTION (in ng) FOR ANTHRACENE
OF SYSTEMS i - v (SEE TEXT FOR DESCRIPTION)

Instrument System	Limit of Detection (ng)
i	0.19
ii	0.48
iii	0.18
iv	0.085
v	0.028

substantial difference in the measured limits of detection.[43]

Noise vs. Background Level

In Figure 14, a log-log plot is given of noise vs. background intensity over six orders of magnitude of background made on system v, with a time constant adjusted to 1 s. The slope of the curve varies from ~ 0.6 at low intensities to ~ 0.9 at high intensities, with a prominent transition region around 10^{-8} A. Whether or not 1/f, or fluctuation, noise predominates is a function of photon flux, photocathode efficiency, system bandwidth, and the amount of inherent fluctuation (flicker) in the excitation source. However, the current level at which 1/f noise is observed to become predominant is somewhat an artifact of the experimental system because it depends not only on the factors mentioned above, but also upon the gain (applied voltage) of the photomultiplier tube. Thus, plots such as those in Figure 14 apply only to the systems from which they are obtained and under the specified conditions of source and detector operation. Once obtained, however, they can help determine whether (or how, as discussed below) further improvement in the system is possible or cost effective.

Origin of Limiting Noise

The limiting background and peak-to-peak noise had typical values of 2×10^{-10} A and 2×10^{-11} A, respectively. These values are about two orders of magnitude greater than those obtained when the PM shutter was open and the source blocked.

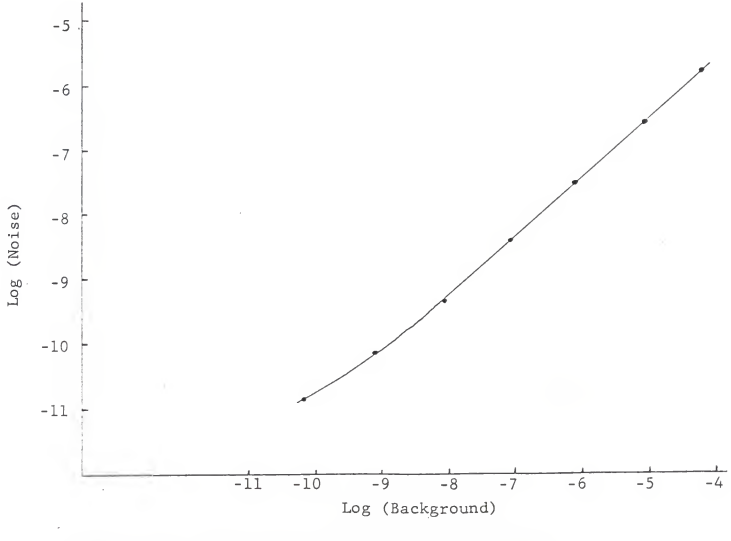

Figure 14. Plot of Log Noise vs. Log Background

Thus, it is seen that the limiting background and noise must originate at the excitation source.

There are three most likely mechanisms which separately or in combination could give rise to the observed background:

(1) UV light of wavelength, λ_{ex}, from the excitation monochromator being scattered by the sample cell and passing through the emission monochromator to the detector.

(2) UV excited sample cell fluorescence.

(3) Stray visible light of wavelength, λ_{em}, from the excitation monochromator being scattered by the sample cell and passed through the emission monochromator to the detector.

Mechanism (1) is unlikely because the setting of the emission monochromator is usually different from λ_{ex} by several times its spectral bandpass and because λ_{ex} is usually well below the range of frequencies passed by the envelope of the PM tube, i.e., a glass envelope in the Hamamatsu 1P21 photomultiplier tube.

Mechanism (2) is more likely than mechanism (1), but it should be of minimal importance if high quality quartz is used to make the sample cell.

Mechanism (3) would seem to be the most likely because a continuum excitation source was used which has a visible spectral irradiance 3 to 10 times greater than its UV spectral irradiance.

Table VIII shows the background signal levels from the

detector with and without an interference filter in the excitation path, anterior to the sample cell. It can be seen from the data that placing the filter in the excitation path decreases the signal level by a factor almost equal to the transmittance of the filter at λ_{em}.

From this, it is concluded that the third mechanism is the most important because it depends (in agreement with the data in Table VIII) on the flux of stray light of wavelength λ_{em} reaching the sample cell. The first two mechanisms (in contradiction to the data in Table III) depend upon the flux of the exciting light reaching the sample cell. In fact, somewhat more than 90% of the background can be attributed to mechanism (3).

Thus, the analyte signal depends upon the flux of the exciting light reaching the cell, while the limiting background and noise depend upon the amount of stray light reaching the cell. There are several general conclusions which can now be drawn about improving the signal-to-noise ratio and limits of detection obtainable with the present system.

For the case where background shot noise predominates:

(i) Any change in the system which increases the flux of exciting light reaching the cell will improve the S/N so long as any concomitant increase in the flux of stray light reaching the cell is less than the square of the increase in exciting light flux.

(ii) Any change in the system which decreases the flux of stray light reaching the cell will improve the

TABLE VIII
BACKGROUND SIGNAL LEVEL WITH AND WITHOUT
INTERFERENCE FILTER IN EXCITATION PATH
PRIOR TO SAMPLE CELL

Conditions	Excitation Monochromator Setting (nm)[a]	Signal (A)
No Filter	235	5.8×10^{-8}
	255	6.9×10^{-8}
	275	5.3×10^{-8}
Filter[b]	235	4.6×10^{-9}
	255	5.7×10^{-9}
	275	4.4×10^{-9}

[a] Emission monochromator set at 370 nm.

[b] Transmittance of filter is 9% at 370 nm and 0.01% at λ_{ex}.

S/N so long as any concomitant decrease in the flux of exciting light reaching the cell is less than the square root of the decrease in stray light flux.

For the case where background flicker noise predominates:

(iii) Any change in the system which increases the flux of exciting light reaching the cell will improve the S/N so long as any concomitant increase in stray light flux reaching the cell is less than the increase in exciting light flux.

(iv) Any change in the system which decreases the flux of stray light reaching the cell will improve the S/N so long as any concomitant decrease in exciting light flux is less than the decrease in stray light flux.

From conclusions (i) and (ii), it would seem that when shot noise predominates, it would be easier to improve the S/N by changing the system so that there is an increase in the flux of exciting light. From conclusions (iii) and (iv), it would seem that when flicker noise predominates, any change in the system which increases the ratio of exciting light flux to stray light flux will improve the S/N regardless of whether the exciting light flux increases or decreases.

There are also a few conclusions which can be made for the case where both analyte signal and background (noise) depend upon the flux of exciting light reaching the sample cell (i.e., mechanisms (1) and (2)). When shot noise predominates, the S/N is directly proportional to the exciting light

flux, and the S/N can improve only if that flux is increased. When flicker noise predominates, there is probably no way to improve the S/N, with the possible exception of using a pulsed source-gated detector system with time resolution (assuming any cell fluorescence has a shorter lifetime than analyte fluorescence).[55] The improvement in S/N gained may not, however, justify the added cost and complexity of such a system.

Finally, the general conclusions discussed above imply that there are practical ways to improve the performance of the gas phase fluorescence detection systems described above. One way would be to use highly intense, stable sources, such as flash lamp pumped dye lasers with good outputs between 200 - 300 nm, where many polynuclear aromatic arenes absorb strongly. Another way would be to use improved optical systems, such as monochromators with holographically produced grating, blazed to be most efficient in the far UV and having relatively lower levels of stray light.

CHAPTER V
CONCLUSIONS

It has been shown in this manuscript that the SIT is capable of limits of detection which are within an order of magnitude of the limits of detection achievable with a typical photomultiplier tube, at least for the cases of gas phase or condensed phase molecular luminescence. These results are in good agreement with the general expectations arising from theoretical considerations of image devices and photomultiplier tubes as detectors in luminescence spectroscopy.

With improvements in image device technology, the difference between photomultiplier tube and image device detectabilities may narrow considerably. In addition, an increase in the length (to several inches) of active target surface of image devices would enhance their multichannel advantage and make them more attractive as detectors for atomic spectroscopy.

It has also been seen that there is a possibility of increasing the detectability of fluorescence detectors for (gas) chromatography by improving the instrumentation (spectrometer) used. This improvement in detectability would hold regardless of whether photomultiplier tubes or image devices were used as detectors.

The decision on whether to use a photomultiplier tube or

image device as a (luminescence) detector should be based on several factors including cost, detectability needed, available analysis time, and amount of information desired. If cost is a prime consideration, the photomultiplier tube system is first choice, as would be the case if maximum detectability were most important. However, as the (spectral) information increases and/or as the amount of time available in which to gather the desired information decreases, then image device systems become more and more attractive.

Similar considerations arise when considering whether fluorescence detectors will find as widespread a use in gas chromatography as they have in liquid chromatography. Their sensitivity, selectivity, and (with image devices) multichannel advantage must be weighed against their nonuniversality, expense (especially with image devices), and increased complexity (compared to that of fluorescence LC detectors).

The use of minicomputers would add greater flexibility and power (e.g., larger dynamic range) to the data collecting and processing capabilities of image devices. The use of (UV) lasers as excitation sources should result in improved limits of detection by increasing the signal level (due to increased absorbtivity of many compounds in the UV) and/or by decreasing the magnitude of stray light.

APPENDIX A
S/N IN TERMS OF CURRENTS

The data of interest to the user of commercial image devices is in the form of counts rather than in the form of currents (or counting rates). Nevertheless, much commercial literature and some research articles give the signal-to-noise ratio of image devices in terms of currents, i.e.,

$$(S/N)_{image} = \frac{i_L}{\overline{\Delta i_T}} \qquad (A1)$$

where i_L is the signal current due to the analyte luminescence and $\overline{\Delta i_T}$ is the total noise current due to all sources. These currents represent the rate at which charge is read from the target during any one individual scan. The magnitudes of i_L and $\overline{\Delta i_T}$ depend upon the amount of charge stored on the target from one readout to the next and on the time it takes to read out the accumulated charge during each scan, and not on how many scans are made.

However, some readers may infer from various articles that if the number of scans is increased by a factor of n_s, then the signal current i_L is also increased by the same factor to $n_s i_L$, and the noise current is increased from $\overline{\Delta i_T}$ to $\sqrt{n_s}\overline{\Delta i_T}$. The fallacy of this argument is two-fold: (1) As seen above, increasing the number of scans increases the total charge or

counts accumulated but has nothing to do with the rate at which the charge (counts) is read out, i.e., current. (2) If the current noise increases by $\sqrt{n_s}$ then the implicit assumption is that the noise is random noise and not proportional noise (such as flicker or whistle). As will be seen below, even though $\overline{\Delta i_T}$ does not depend upon the number of scans, it does depend upon the exposure time (the time between scans). Therefore $\overline{\Delta i_T}$ will depend upon t_d and n_d as well.

At any rate, most users of image devices are interested primarily in the signal-to-noise characteristics of the total number of counts (equivalent to the total charge accumulated) in memory rather than in the signal-to-noise characteristics of the rate (current) at which charge is transferred from the target and stored in memory (in the form of counts); and such (current) information, even when available is seldom of use to the analytical spectroscopist performing the measurements.

Regardless, in order to complete the discussion undertaken in this paper, and hopefully to prevent some confusion by others, eq. (A2) gives a signal-to-noise expression in terms of currents. The expression for the signal-to-noise ratio is

$$(S/N)_{image} = i_L/\{\sqrt{(\overline{\Delta i}^2_{LS_i} + 2\overline{\Delta i}^2_{BS_i} + 2\overline{\Delta i}^2_{IS_i} + 2\overline{\Delta i}^2_{SS_i} + 2\overline{\Delta i}^2_{DS_i}) + (\overline{\Delta i}_{LF_i} + 2\overline{\Delta i}_{IF_i} + 2\overline{\Delta i}_{SF_i})^2 + 4\overline{\Delta i}^2_{BF_i} + 8\overline{\Delta i}^2_{DF_i} + 4\overline{\Delta i}^2_{A}}\} \quad \text{(A2)}$$

where:

The numerical coefficients of the different terms result from the same experimental measurement considerations given in the discussion of equation (5);

$\overline{\Delta i}_{XS_i}$ represents the shot (rms) noise current due to process X in channel i, A;

$\overline{\Delta i}_A$ represents the preamplifier noise current, A;

$\overline{\Delta i}_{XF_i}$ represents the proportional (mainly flicker) noise current due to process X in channel i, A.

The value of signal-to-noise obtained using this expression will be smaller than the value obtained using the count expression (equations (5), (6), (7), if $n_s > 1$). The current terms in equation (A2) can be expressed in terms of the operating parameters of an image device as follows:

$$i_{X_i} = \frac{eq_i G A_i E_{X_i} t_e}{t_r} \qquad \text{(A3)}$$

where:

e = charge of electron, C;

q_i = photon to photoelectron conversion efficiency of the photocathode, dimensionless;

G = gain of device, dimensionless

E_{X_i} = photon irradiance, photons cm^{-2} s^{-1};

t_s = scan time, s;

t_e = exposure time, s ($t_e = t_s + t_d n_d$, with t_d, n_d as defined earlier);

t_r = readout time of channel i, s;

A_i = area of channel i, cm^2.

$$\overline{\Delta i}_{XS_i} = \sqrt{2e\Delta f i_{X_i}} \qquad \text{(A4)}$$

where:

Δf = frequency response bandwidth of measurement system ($\Delta f = f_u - f_l$ or $\sim 1/2t_a$, where t_a is the averaging time of the system), Hz;

i_{X_i} = current given in equation (A3) from a photon induced process, or from dark current, A;

$$\overline{\Delta i}_{XF_i} = \xi_{X_i} i_{X_i} \qquad \text{(A5)}$$

where:

ξ_{X_i} = flicker (fluctuation) constant for process X in channel i, dimensionless;

$$\overline{\Delta i}_A = \frac{\bar{n}_p e}{t_r} \qquad \text{(A6)}$$

where:

$\bar{n}_p$ = the equivalent target electron uncertainty per channel (for PAR/OMA, it is $\sim$2500 rms electrons per channel), dimensionless.

The signal-to-noise expression in terms of current for a photomultiplier (non-integrating) detector yields the same results as the signal-to-noise expression in terms of counts (or count rates) and so will not be given here. It should be noted that the analogs of equations (A2), (A3), (A4), and (A5) for the PM differ from the ones in the text in that the sub i's

are omitted. In addition, for the PM analog of equation (A3), $t_e/t_r = 1$; and there is no analog to equation (A6) because $\overline{\Delta I}_A$ is or can "always" be made negligible for PM.

APPENDIX B
DEFINITIONS, TERMS, AND UNITS WITH IMAGE DEVICES

Preamplifier noise for image device systems is often recorded in terms of rms counts (or electrons) per channel per frame (scan). It should be stressed that the designation of 1 count (~2500 electrons for PAR/OMA system) per channel per frame is an rms noise count rate and not a signal count rate.

Dark currents for image devices are listed typically either as currents, readout count rates, or electron fluxes. Several calculations of dark current magnitudes (for the PAR/OMA system) will be given which illustrate among other things, that care must be taken to distinguish between the rate at which dark current charge accumulates, and the rate at which it is read out from the V, SEC, SIT, ISIT target.

(i) If the dark current read out for the entire image device is 8×10^{-9} A, then assuming a 500 channel device, the conversion to dark current in terms of the number of counts accumulating (on the target surface) per channel per second is given by:

$$8\times10^{-9}\ \frac{C}{s} \times \frac{1\ \text{electron}}{1.6\times10^{-19}\ C} \times \frac{1}{500\ \text{channel}} \times \frac{32.8\times10^{-6}\ s}{\text{readout}}$$

$$\times \frac{1\ \text{readout}}{\text{accumulation}} \times \frac{1\ \text{accumulation}}{32.8\times10^{-3}\ s} \times \frac{1\ \text{count}}{2500\ \text{electrons}}$$

$$= \frac{40\ \text{counts}}{\text{channel}\ s}$$

(ii) The conversion from a readout count rate to an accumulation count rate is perfomed similarly, i.e., assuming a readout count rate of 4.0×10^4 counts channel^{-1} s^{-1}, then the accumulation rate is given by:

$$4.0\times10^4 \frac{\text{counts}}{\text{channel s}} \times \frac{32.8\times10^{-6}\ \text{s}}{\text{readout}} \times \frac{1\ \text{readout}}{\text{accumulation}}$$

$$\times \frac{1\ \text{accumulation}}{32.8\times10^{-3}\ \text{s}} = \frac{40\ \text{counts}}{\text{channel s}}$$

(iii) A readout electron flux of 8×10^{10} electrons cm^{-2} s^{-1} can be converted to an accumulation rate (counts channel^{-1} s^{-1}) as follows:

$$8\times10^{10} \frac{\text{electrons}}{\text{cm}^2\ \text{s}} \times \frac{12.8\times10^{-4}\ \text{cm}^2}{\text{channel}} \times \frac{32.8\times10^{-6}\ \text{s}}{\text{readout}}$$

$$\times \frac{1\ \text{readout}}{\text{accumulation}} \times \frac{1\ \text{accumulation}}{32.8\times10^{-3}\ \text{s}} \times \frac{1\ \text{count}}{2500\ \text{electrons}}$$

$$= \frac{40\ \text{counts}}{\text{channel s}}$$

The above calculations are meant only to illustrate the procedure used to interconvert the various literature values for dark count rate. The author does not imply, or mean to imply that the values chosen in the examples above are the actual values for any specific image devices.

Fixed pattern noises do exist with image devices and have been given names such as coherent noise, hash noise, sinusoidal noise, etc. These noises seem to depend to a great extent on the specific instrument used (its adjustment, ground-

ing, and so forth). As a result, such noises are difficult to characterize in terms of mathematical expressions. Therefore, even though these noises can become the limiting noises (under conditions of low light flux measured for periods of a few seconds or less) when the instrument has not been set up and adjusted optimally, they have not been considered in this discussion.

REFERENCES

1. Y. Talmi, Anal. Chem., 47, 685A (1975).
2. Ibid., 47, 697A (1975).
3. K. W. Busch, N. G. Howell, and G. H. Morrison, Anal. Chem., 46, 575 (1974).
4. Ibid., 46, 1231 (1974).
5. Ibid., 46, 2074 (1974).
6. N. G. Howell, J. D. Ganjei, and G. H. Morrison, Anal. Chem., 48, 319 (1976).
7. J. D. Ganjei, N. G. Howell, J. R. Roth, and G. H. Morrison, Anal. Chem., 48, 505 (1976).
8. M. J. Milano, H. L. Pardue, T. E. Cook, R. E. Santini, D. H. Margerum, and J. M. T. Raycheba, Anal. Chem., 46, 374 (1974).
9. A. Danielson, P. Lindblum, and E. Suderman, Chem. Scripta, 6, 5 (1974).
10. A. Danielson and P. Lindblum, Phys. Scripta, 5, 227 (1974).
11. D. L. Wood, A. B. Dargis, and D. L. Nash, Appl. Spectrosc., 27, 310 (1975).
12. G. Horlick and E. G. Codding, Anal. Chem., 45, 1490 (1973).
13. E. G. Codding and G. Horlick, Appl. Spectrosc., 27, 366 (1973).
14. Ibid., Spectrosc. Letters, 7, 33 (1974).
15. G. Horlick, E. G. Codding, and S. T. Leung, Appl. Spectrosc., 29, 48 (1975).
16. J. A. C. Broekaert, Bull. Soc. Chim. Belg., 84, 1159 (1975).
17. F. L. Fricke, O. Rose, and J. A. Caruso, Anal. Chem., 47, 2018 (1975).

18. D. O. Knapp, N. Omenetto, F. W. Plankey, and J. D. Winefordner, Anal. Chim. Acta, 69, 455 (1974).

19. T. L. Chester, H. Haraguchi, D. O. Knapp, J. D. Messman, and J. D. Winefordner, Appl. Spectrosc., 30, 410 (1976).

20. K. W. Jackson, K. M. Aldous, and D. G. Mitchell, Spectrosc. Letters, 6, 315 (1973).

21. Ibid., Appl. Spectrosc., 28, 569 (1974).

22. K. M. Aldous, D. G. Mitchell, and K. W. Jackson, Anal. Chem., 47, 1034 (1975).

23. G. Horlick and E. G. Codding, Appl. Spectrosc., 29, 167 (1975).

24. Ibid., Anal. Chem., 46, 133 (1974).

25. M. J. Milano and H. L. Pardue, Anal. Chem., 47, 25 (1975).

26. G. Horlick and E. G. Codding, Anal. Chem., 46, 133 (1974).

27. T. E. Cook, M. J. Milano, and H. L. Pardue, Clin. Chem., 20, 1422 (1974).

28. M. J. Milano and H. L. Pardue, Clin. Chem., 21, 211 (1975).

29. T. E. Cook, H. L. Pardue, and R. E. Santini, Anal. Chem., 48, 452 (1976).

30. T. A. Nieman and C. G. Enke, Anal. Chem., 48, 619 (1976).

31. D. A. Yates and T. Kuwana, Anal. Chem., 48, 510 (1976).

32. T. A. Nieman, F. J. Holler, and C. G. Enke, Anal. Chem., 48, 899 (1976).

33. R. E. Dessy, W. G. Nunn, C. A. Titus, and R. Reynolds, J. Chromatog. Sci., 14, 195 (1976).

34. I. M. Warner, J. B. Callis, E. R. Davidson, and G. D. Christian, Clin. Chem., 22(9), 1483 (1976).

35. T. Vo-Dinh, D. J. Johnson, and J. D. Winefordner, Spectrochim. Acta A, submitted.

36. R. P. Cooney, T. Vo-Dinh, and J. D. Winefordner, Anal. Chim. Acta, in press

37. W. H. Woodruff and G. H. Atkinson, Anal. Chem., 48, 186 (1976).

38. R. E. Santini, M. J. Milano, and H. L. Pardue, Anal. Chem., 45, 915A (1973).

39. D. G. Mitchell, K. W. Jackson, and K. M. Aldous, Anal. Chem., 45, 1215A (1973).

40. K. W. Busch and G. H. Morrison, Anal. Chem., 45, 712A (1973).

41. J. D. Winefordner, J. J. Fitzgerald, and N. Omenetto, Appl. Spectrosc., 29, 369 (1975).

42. M. C. Bowman and M. Beroza, Anal. Chem., 40, 535 (1968).

43. H. P. Burchfield, R. J. Wheeler, and J. B. Bernos, Anal. Chem., 43, 1976 (1971).

44. H. P. Burchfield, E. E. Green, R. J. Wheeler, and S. M. Billedeau, J. of Chromatography, 99, 697 (1974).

45. D. J. Freed and L. R. Faulkner, Anal. Chem., 44, 1194 (1972).

46. J. W. Robinson and J. P. Goodbread, Anal. Chim. Acta, 66, 239 (1973).

47. I. M. Warner, J. B. Callis, E. R. Davidson, M. Gouterman, and G. D. Christian, Anal. Letters, 8, 665 (1975).

48. T. Vo-Dinh, D. J. Johnson, and J. D. Winefordner, to be published.

49. R. E. Dessy, W. G. Hann, C. A. Titus, and W. R. Reynolds, J. Chromatog. Sci., 14, 195 (1976).

50. S. Udenfriend, "Fluorescence Assay in Biology and Medicine," pp. 568-572, Academic Press, NY (1969).

51. E. J. Bair, "Introduction to Chemical Instrumentation," McGraw-Hill, NY, (1962).

52. J. D. Winefordner, V. Svoboda, and L. J. Cline, CRC Critical Rev. Anal. Chem., 1, 233 (1970).

53. T. L. Chester and J. D. Winefordner, Anal. Chem., submitted.

54. J. D. Winefordner, R. Avni, T. L. Chester, J. J. Fitzgerald, L. P. Hart, D. J. Johnson, and F. W. Plankey, Spectrochim. Acta, 31B, 1 (1976).

55. G. D. Boutilier, J. D. Bradshaw, S. J. Weeks, and J. D. Winefordner, Appl. Spectrosc., submitted.

56. R. J. Perchalski, J. D. Winefordner, and B. J. Wileler, Anal. Chem., 47, 1993 (1975).

57. T. C. O'Haver and J. D. Winefordner, J. Chem. Ed., 46, 241 (1969).

58. D. J. Johnson, W. K. Fowler, and J. D. Winefordner, submitted.

59. M. Margoshes, Spectrochim. Acta, 25B, 113 (1970).

60. M. Margoshes, Pittsburgh Conference on Analytical Chemistry and Applied Spectroscopy, 1970.

61. D. O. Knapp, Ph. D. Thesis, University of Florida, Gainesville, FL, 1973.

62. H. V. P. Klochkov and A. M. Makushenko, Opt. Spectrosc., 15, 25 (1963).

63. E. D. Pellizzari and C. M. Sparacino, Anal. Chem., 45, 378 (1973).

64. J. D. Winefordner, ed., "Trace Analysis, Spectroscopic Methods for Elements," John Wiley, NY (1976).

BIOGRAPHICAL SKETCH

Ray Cooney was born, somewhat prematurely, on August 24, 1947, in Evanston, Illinois. He attended grade and high schools in the Chicago area and received a B. S. degree from the University of Illinois in 1969. Since that time he has (among other things) been pursuing his Ph. D. degree at the University of Florida.

I certify that I have read this study and that in my opinion it conforms to acceptable standards of scholarly presentation and is fully adequate, in scope and quality, as a dissertation for the degree of Doctor of Philosophy.

James D. Winefordner, Chairman
Graduate Research Professor of Chemistry

I certify that I have read this study and that in my opinion it conforms to acceptable standards of scholarly presentation and is fully adequate, in scope and quality, as a dissertation for the degree of Doctor of Philosophy.

Roger F. Bates
Professor of Chemistry

I certify that I have read this study and that in my opinion it conforms to acceptable standards of scholarly presentation and is fully adequate, in scope and quality, as a dissertation for the degree of Doctor of Philosophy.

Willis B. Person
Professor of Chemistry

I certify that I have read this study and that in my opinion it conforms to acceptable standards of scholarly presentation and is fully adequate, in scope and quality, as a dissertation for the degree of Doctor of Philosophy.

Paul Urone
Professor of Environmental Engineering

I certify that I have read this study and that in my opinion it conforms to acceptable standards of scholarly presentation and is fully adequate, in scope and quality, as a dissertation for the degree of Doctor of Philosophy.

Gerhard M. Schmid
Associate Professor of Chemistry

This dissertation was submitted to the Graduate Faculty of the Department of Chemistry in the College of Arts and Sciences and to the Graduate Council, and was accepted as partial fulfillment of the requirements for the degree of Doctor of Philosophy.

March, 1977

Dean, Graduate School